The braincase anatomy of *Simosaurus gaillardoti* (Diapsida: Sauropterygia) revealed with X-Ray micro-Computed Tomography (#114520)

First submission

Guidance from your Editor

Please submit by **22 Mar 2025** for the benefit of the authors (and your token reward) .

Structure and Criteria
Please read the 'Structure and Criteria' page for guidance.

Author notes
Have you read the author notes on the guidance page?

Raw data check
Review the raw data.

Image check
Check that figures and images have not been inappropriately manipulated.

If this article is published your review will be made public. You can choose whether to sign your review. If uploading a PDF please remove any identifiable information (if you want to remain anonymous).

Files
Download and review all files from the materials page.

12 Figure file(s)

Structure and Criteria

Structure your review

The review form is divided into 5 sections. Please consider these when composing your review:

1. **BASIC REPORTING**
2. **EXPERIMENTAL DESIGN**
3. **VALIDITY OF THE FINDINGS**
4. General comments
5. Confidential notes to the editor

You can also annotate this PDF and upload it as part of your review

When ready submit online.

Editorial Criteria

Use these criteria points to structure your review. The full detailed editorial criteria is on your guidance page.

BASIC REPORTING

- Clear, unambiguous, professional English language used throughout.
- Intro & background to show context. Literature well referenced & relevant.
- Structure conforms to PeerJ standards, discipline norm, or improved for clarity.
- Figures are relevant, high quality, well labelled & described.
- Raw data supplied (see PeerJ policy).

EXPERIMENTAL DESIGN

- Original primary research within Scope of the journal.
- Research question well defined, relevant & meaningful. It is stated how the research fills an identified knowledge gap.
- Rigorous investigation performed to a high technical & ethical standard.
- Methods described with sufficient detail & information to replicate.

VALIDITY OF THE FINDINGS

- **Impact and novelty is not assessed.** Meaningful replication encouraged where rationale & benefit to literature is clearly stated.
- All underlying data have been provided; they are robust, statistically sound, & controlled.
- Conclusions are well stated, linked to original research question & limited to supporting results.

Standout reviewing tips

The best reviewers use these techniques

Tip	*Example*
Support criticisms with evidence from the text or from other sources	*Smith et al (J of Methodology, 2005, V3, pp 123) have shown that the analysis you use in Lines 241-250 is not the most appropriate for this situation. Please explain why you used this method.*
Give specific suggestions on how to improve the manuscript	*Your introduction needs more detail. I suggest that you improve the description at lines 57- 86 to provide more justification for your study (specifically, you should expand upon the knowledge gap being filled).*
Comment on language and grammar issues	*The English language should be improved to ensure that an international audience can clearly understand your text. Some examples where the language could be improved include lines 23, 77, 121, 128 – the current phrasing makes comprehension difficult. I suggest you have a colleague who is proficient in English and familiar with the subject matter review your manuscript, or contact a professional editing service.*
Organize by importance of the issues, and number your points	*1. Your most important issue* *2. The next most important item* *3. …* *4. The least important points*
Please provide constructive criticism, and avoid personal opinions	*I thank you for providing the raw data, however your supplemental files need more descriptive metadata identifiers to be useful to future readers. Although your results are compelling, the data analysis should be improved in the following ways: AA, BB, CC*
Comment on strengths (as well as weaknesses) of the manuscript	*I commend the authors for their extensive data set, compiled over many years of detailed fieldwork. In addition, the manuscript is clearly written in professional, unambiguous language. If there is a weakness, it is in the statistical analysis (as I have noted above) which should be improved upon before Acceptance.*

The braincase anatomy of *Simosaurus gaillardoti* (Diapsida: Sauropterygia) revealed with X-Ray micro-Computed Tomography

Elisa H London [1], **Dennis FAE Voeten** [2, 3], **Torsten M Scheyer** [Corresp., 4], **Henning Blom** [5]

[1] Department of Earth Sciences, Uppsala Universitet, Uppsala, Sweden

[2] Frisian Museum of Natural History, Leeuwarden, Netherlands

[3] Vertebrate Evolution, Development and Ecology group, Naturalis Biodiversity Center, Leiden, Netherlands

[4] Department of Paleontology, University of Zurich, Zurich, Switzerland

[5] Department of Organismal Biology, Uppsala Universitet, Uppsala, Sweden

Corresponding Author: Torsten M Scheyer
Email address: tscheyer@pim.uzh.ch

Sauropterygia is a clade of Mesozoic marine reptiles that includes the eosauropterygian *Simosaurus gaillardoti* Meyer, 1842, classically considered to be a member of Nothosauroidea. The braincase of this species has thus far only been studied in acid-prepared specimens. Acid preparation is a destructive technique prone to information loss, e.g. through the dissolution of thin braincase bones. Here, one well-preserved skull (SMNS 16363) that remains partially embedded in matrix has been visualised using X-ray micro-Computed Tomography and the braincase region has been virtually extracted. This braincase provides valuable information on the general shape of the endocast, the existence and shape of epipterygoids, which were previously considered absent in the taxon, the course of cranial nerves, and the bifurcation of the internal carotid arteries along an expanded and broad parabasisphenoid, the latter extending in a tapering cultriform process to the level of the external and internal narial openings. The arrangement of the semicircular canals of the inner ear confirms previously hypothesised adaptations for near-shore aquatic life in the species. The similarities of the braincase anatomy of *Simosaurus gaillardoti* and *Nothosaurus marchicus* support the current phylogenetic placement of the former as an early branching member of Nothosauroidea. The cranial flattening observed in nothosaurs relative to the less dorsoventrally flattened skull of *Simosaurus* reflects diverging feeding strategies. Most nothosaurs were fish-trap ambush predators whereas *Simosaurus gaillardoti* had durophagous, as well as (opportunistic) piscivorous capacities. These results indicate that specialised piscivorous predation using fish-trap dentition could be independently derived in nothosaurs and in pistosauroids (including plesiosaurs).

The braincase anatomy of *Simosaurus gaillardoti* (Diapsida: Sauropterygia) revealed with X-Ray micro-Computed Tomography

Elisa H. London[1], Dennis F. A. E. Voeten[2,3], Henning Blom[4], Torsten M. Scheyer[5]

[1] Department of Earth Sciences, Uppsala University, Villavägen 16, 752 36 Uppsala, Sweden
[2] Frisian Museum of Natural History, Schoenmakersperk 2, 8911 EM Leeuwarden, The Netherlands
[3] Vertebrate Evolution, Development and Ecology group, Naturalis Biodiversity Center, Postbus 9517, 2300 RA Leiden, The Netherlands
[4] Department of Organismal Biology, Uppsala University, Evolutionsbiologiskt Centrum EBC, Norbyvägen 18 A, 752 36 Uppsala, Sweden
[5] Department of Paleontology, University of Zurich, Karl Schmid-Strasse 4, CH-8006 Zurich, Switzerland

Corresponding Author:
Torsten M. Scheyer[5]
Karl Schmid-Strasse 4, Zurich, 8006, Switzerland
Email address: tscheyer@pim.uzh.ch

Abstract

Sauropterygia is a clade of Mesozoic marine reptiles that includes the eosauropterygian *Simosaurus gaillardoti* Meyer, 1842, classically considered to be a member of Nothosauroidea. The braincase of this species has thus far only been studied in acid-prepared specimens. Acid preparation is a destructive technique prone to information loss, e.g. through the dissolution of thin braincase bones. Here, one well-preserved skull (SMNS 16363) that remains partially embedded in matrix has been visualised using X-ray micro-Computed Tomography and the braincase region has been virtually extracted. This braincase provides valuable information on the general shape of the endocast, the existence and shape of epipterygoids, which were previously considered absent in the taxon, the course of cranial nerves, and the bifurcation of the internal carotid arteries along an expanded and broad parabasisphenoid, the latter extending in a tapering cultriform process to the level of the external and internal narial openings. The arrangement of the semicircular canals of the inner ear confirms previously hypothesised

adaptations for near-shore aquatic life in the species. The similarities of the braincase anatomy of *Simosaurus gaillardoti* and *Nothosaurus marchicus* support the current phylogenetic placement of the former as an early branching member of Nothosauroidea. The cranial flattening observed in nothosaurs relative to the less dorsoventrally flattened skull of *Simosaurus* reflects diverging feeding strategies. Most nothosaurs were fish-trap ambush predators whereas *Simosaurus gaillardoti* had durophagous, as well as (opportunistic) piscivorous capacities. These results indicate that specialised piscivorous predation using fish-trap dentition could be independently derived in nothosaurs and in pistosauroids (including plesiosaurs).

Introduction

Sauropterygia is a diverse clade of marine reptiles that lived from the Lower Triassic until the K-Pg mass extinction (c. 252 – 66 Ma) (Rieppel, 2000; Scheyer et al., 2014), but recent studies pushed back the possible appearance of marine reptile clades, including the sauropterygians, to the end of the Permian (Wang et al., 2022; Kear et al., 2023, 2024). Sauropterygia is generally considered to include the two clades Placodontiformes and Eosauropterygia (Fig. 1A-C), although there is an ongoing discussion on the internal topology of the tree and the systematics are far from stable. Some studies divide Eosauropterygia into Pachypleurosauria, Pistosauroidea, and Nothosauroidea (e.g., Scheyer et al., 2017; Allemand et al., 2023). Saurosphargidae was recently added to the phylogenetic analysesas well, but its position either within or closely related to Sauropterygia remains contested (e.g., Wang et al., 2022; Wolniewicz et al., 2023). Placodontiformes appeared in the early Anisian (247-242 Ma) in nearshore environments Placodontia in particular featured a highly modified dentition specialised with flat and broad plate-like teeth facilitating their durophagous diet (Rieppel, 2002; Neenan et al., 2013, 2015; Pommery et al., 2021; Laboury et al., 2023). Arguably the best-understood placodontoid genus, including the skull- and braincase anatomy, is *Placodus* Agassiz, 1833, known from numerous isolated bones and teeth but also associated skeletons (e.g., Agassiz, 1833-1845; Drevermann, 1933; Jiang et al., 2010; Nosotti & Rieppel, 2002; Jiang et al., 2008; Neenan & Scheyer, 2012; Klein et al., 2022). *Placodus* was a bottom feeder, mostly preying on shelled marine invertebrates (Rieppel, 2002; Klein et al., 2015; Xing et al., 2020). Among Eosauropterygia, Pachypleurosauria potentially appeared in the fossil record in the Olenekian (237 – 227 Ma) with taxa such as *Majiashanosaurus discocoracoidis* (Jiang et al. 2014; Wang et al., 2022), but its

placement among Sauropterygia has also been contested, as it was also found outside of Eosauropterygia (Wolniewicz et al., 2023), or as successive sister taxon (with *Hanosaurus*) to Nothosauroidea plus Pachypleurosauria (Li and Liu, 2020). Pachypleurosauria sensu stricto mostly fed on small, soft-bodied animals (Rieppel, 2002) and the majority of pachypleurosaurs are equipped with teeth consisting of a single dental morphology: small, conical teeth suited for processing soft-bodied invertebrates and fish (Rieppel, 2002). Facultatively durophagous forms are also known as is evidenced by *Anarosaurus heterodontus* (Klein, 2009). Pistosauroidea, which in the Late Triassic gave rise to the globally distributed open-water plesiosaurs including the genus *Plesiosaurus*, were piscivorous (Storrs, 1993; Wintrich et al., 2017).

Nothosauroidea includes Olenekian forms that are among the oldest currently recognised sauropterygian fossils (Li & Liu, 2020; Scheyer et al., 2019; Kear et al., 2024). Nothosaurs are mostly found in coastal or platform deposits and are considered piscivorous but potentially include the more durophagous *Simosaurus* (Storrs, 1993; Rieppel, 1999, 2002; Klein & Griebeler, 2018).

The family Simosauridae contains two species in monospecific genera: *Simosaurus gaillardoti* (Rieppel, 2000; De Miguel Chaves et al., 2018a; Fig. 1D-F) and *Paludidraco multidentatus* (De Miguel Chaves et al., 2018b). *P. multidentatus* is a relatively recently discovered simosaurid that was described based on one specimen found in the Keuper facies in central Spain dating from the Carnian to Norian (237 – 208 Ma) (De Miguel Chaves et al., 2018b). *S. gaillardoti* appeared in the Ladinian stage (242 – 237 Ma) and disappeared in the Carnian stage (237 – 227 Ma) (Rieppel, 2000; Dalla Vecchia, 2008; Klein et al., 2016; De Miguel Chaves et al., 2018a). The species can be found in Upper Muschelkalk and Lower Keuper stratigraphic units of mostly the western Tethyan region (e.g., Klein et al., 2016) but has also been described in the Middle East (Kear et al., 2010; Cabezuelo-Hernández et al., 2024). The phylogenetic position of *S. gaillardoti* remains debated, with most older studies classifying it as a nothosauroid (Fig. 1) despite distinct morphological differences from other nothosauroids (Cheng et al., 2016; Klein et al., 2016; De Miguel Chaves et al., 2018a; highly nested within Nothosauroidea as sister taxon to *Germanosaurus*: Li & Liu, 2020). Other recent studies found Simosauridae (i.e., *Simosaurus* and *Paludidraco*) as sister clade to Nothosauridae plus Pistosauroidea (Wang et al., 2022) or *Simosaurus* as the sister taxon to Pistosauridae (Qiao et al., 2022; Wolniewicz et al., 2023; note that other nothosaurs were not included in those studies).

Simosaurus gaillardoti could reach 3-4 meters in body length. Its skulls are flat and brevirostrine, meaning they feature a broad jaw with a short rostrum (Rieppel, 1994b). *S. gaillardoti* crania have been shown to exhibit relatively large variation (Rieppel, 1994a; De Miguel Chaves et al., 2018a). This variation, is for example, expressed in the structural openings on the dorsal side of the skull (De Miguel Chaves et al., 2018a). Compared to other nothosaurs, *Simosaurus* has large, rounded upper temporal fenestra (Fig. 1, 2). Some nothosaurs have a specialised (mostly size-related) piercing dentition with large stout and often strongly recurved fangs followed by small, more gracile and often less-curved teeth (e.g., Rieppel, 2000). This has been interpreted to facilitate ensnaring or trapping fish within the jaws, rather than piercing them (Rieppel, 2002; Laboury et al., 2023). *S. gaillardoti,* on the other hand, has teeth that are slightly bulbous in shape and more similarly sized (Rieppel 1994a, 2002). This rather suggests a durophagous feeding strategy for *S. gaillardoti* (Rieppel, 2002). Based on its jaw mechanics, it might have been able to execute a strong and quick snapping bite to process ammonoids and hard-scaled fish (Rieppel, 1994a). The simosaurid *P. multidentatus* has teeth that, unlike those of *S. gaillardoti*, appear adapted for filter-feeding (De Miguel Chaves et al., 2018b).

In recent years, visualisation with X-ray micro-Computed Tomography (μCT) has become an increasingly popular instrument for palaeontological investigation, especially to study the internal skull- and braincase anatomy, which are usually not easily accessible (Sutton, 2008). Since μCT scanning is a non-destructive technique that reveals internal structures using density differences in the scans (Germain & Ladevèze, 2021; Leyhr, 2023), this provides improved insight into the morphology and internal anatomy of diverse fossils without damaging or sacrificing rare specimens. Utilisation of μCT scanning thus prevents rare specimens from being destroyed by e.g., acid-preparation (e.g. Rieppel, 1994b) or (serial) thin sectioning (e.g., Klein, 2010), thus conserving them for improved future methods, while the virtual data can be made easily available and shared without the need to handle the often very delicate and fragile specimens (Sutton et al., 2016). The number of scanned sauropterygian skulls, including segmented braincases in publications, remain scarce however (summarised for example in Allemand et al., 2023). Sauropterygian skulls that were scanned with μCT include, for example, *Nothosaurus marchicus* (Voeten et al., 2018), *Hispaniasaurus cranioelongatus* (Marquez-Aliaga et al., 2019), *Keichousaurus hui* (Liao et al., 2021), *Placodus gigas* (Neenan & Scheyer, 2012), *Henodus chelyops* (Pommery et al., 2021), *Parahenodus atancensis* (De Miguel Chaves et al.,

2020), as well as *Dolichorhynchops* sp. (Sato et al., 2011) and *Libonectes morgani* (Allemand et al., 2019). Of the mentioned examples, *H. cranioelongatus* lacks the posterior braincase region, and *H. chelyops* and *K. hui* were so far imaged only for dental evaluation and are thus not associated with a segmented braincase (Marquez-Aliaga et al., 2019; Liao et al., 2021; Pommery et al., 2021). In contrast, braincase and/or endocast descriptions based on CT scan data exist for the plesiosaur *Dolichorhynchops* sp. (Sato et al., 2011) and *Libonectes morgani* (Allemand et al., 2019).

Concerning nothosauroids, Rieppel (1994b) described the anatomy of acid-prepared skulls of *Simosaurus gaillardoti* and *Nothosaurus* sp. Although the acid preparation, a destructive technique, led to a greater understanding of the exterior skull morphology, it failed to capture the comprehensive internal anatomy of *S. gaillardoti* and often thin and fragile bones within the braincase were lost. More recently, the cranial endocast of *Nothosaurus marchicus* (Voeten et al., 2018) was described, but detailed renderings of the braincase bones were not included at the time. The present study aims to describe the braincase anatomy by providing renderings of the well-ossified posterior region of the skull alongside the associated endocranial voids of a *Simosaurus gaillardoti* specimen (Fig. 2A-H; Supplementary Fig. 1) that is still largely covered in sediment matrix. Utilising µCT scan data and 3D reconstruction (also of an additional specimen of *S. gaillardoti*; see Supplementary Fig. 2) are used to explore and interpret the similarities and differences relative to other nothosaurs in their anatomical, morphofunctional, and phylogenetic contexts.

Materials & Methods

The material studied consists of the cranium of *Simosaurus gaillardoti* (SMNS 16363), which was found in the Upper Muschelkalk of Murr, Baden-Württemberg, Germany. The cranium is approximately 38 cm in length and is almost complete, but parts have been reconstructed with plaster for display purposes (Fig. 1D-F; Supplementary Fig. 1). In addition, to verify the morphology of some of the braincase of *Simosaurus*, an additional specimen (GPIT/RE/09313) was partially segmented. This specimen was mostly prepared out of the sediment matrix except the braincase region. The *Simosaurus* cranial scan data were then also compared to published scan data on *Nothosaurus marchicus* (TW480000375; Voeten et al., 2018); *Placodus gigas* (UMO BT 13; Neenan & Scheyer, 2012), and the plesiosaurs *Dolichorhynchops* sp. (ROM

29010; Sato et al., 2011) and *Libonectes morgani* (D1-8213; Allemand et al., 2019). Due to preservational reasons or difficulties related to clear identification of braincase bones, we refrain from making detailed comparisons with the braincase and cranial endocast of *Parahenodus atancensis* and the available CT scan data of *Keichousaurus hui* and *Hispaniasaurus cranioelongatus*.

Institutional abbreviations. D1, collections of the Rhinopolis Museum, Gannat, France; GPIT, Paläontologische Sammlung der Universität Tübingen, Germany; ROM, Royal Ontario Museum, Toronto, Ontario, Canada; SMNS, Staatliches Museum für Naturkunde Stuttgart, Germany; TW, collections of Museum TwentseWelle, Enschede, The Netherlands; UMO, Urwelt-Museum Oberfranken, Bayreuth, Germany.

Anatomical abbreviations. aCerC, cerebral carotid artery; aIC, internal carotid artery; aip, anterior inferior process of prootic; aPAL, palatine artery; aPT; pterygoid artery; asc, anterior semicircular canal; ba, basilar artery; bo, basioccipital; cav.ep, cavum epiptericum; cba, cavity for basilar artery; cbr, cerebellum; cer, cerebrum; clp, clinoid process of parabasisphenoid complex; CN V, passage for trigeminal cranial nerve (V); CN VII hy; passage for hyomandibular branch of facial cranial nerve (CN VII); CN VIII, passage for vestibulocochlear cranial nerve (VIII); CN IX-XI, passage for glossopharyngeal (IX), vagus (X) and accessory cranial nerves (XI); CN XII, passage for hypoglossal cranial nerve (XII); crc, crus commune; cup, cultriform process; cqp, cranio-quadrate passage; en, external narial opening; end, endocast; ept, epipterygoid; ept-fco, pterygoid facet of the epipterygoid; ex, exoccipital; fm, foramen magnum; fo, fenestra ovalis; ju.f, jugular foramen; la, bony labyrinth; lsc, lateral semicircular canal; m, sediment matrix; mds, median septum; mo, medulla oblongata; o, orbit; op, opisthotic; opt, optic lobe; pa, parietal; para/pin, parapineal/pineal complex; parf, parietal foramen; pa-sq, undifferentiated parietal-squamosal; pbs, parabasisphenoid; pi, paracondylar interstices; po, pons; pr, prootic; psc, posterior semicircular canal; pt, pterygoid; ptf, posttemporal fenestra; sin, sinus system; so, supraoccipital; sq, squamosal; stc, sella turcica; utf, upper temporal fenestra; vCL, lateral head vein (=vena capitis lateralis); ve, vestibule.

Data acquisition. Both crania were scanned with a Phoenix v|tome|x L240 machine at the Accès Scientifique à la Tomographie à Rayons X facility (AST-RX) in the Muséum national d'Histoire naturelle (MNHN), Paris, France. Micro-X-ray tomography was used to scan the SMNS 16363 cranium twice, once to image the complete cranium (Fig. 2) and subsequently to obtain a higher-resolution scan of the braincase region. The complete cranium was scanned with a voltage of 160 kV and a current of 500 mA. The acquired voxel size is 0.12739793 mm. The higher-resolution scan of the braincase was scanned with a voltage of 165 kV and a current of 500 mA, and the voxel size is 0.06218133 mm. The second specimen, GPIT/RE/09313, was scanned using 150kV at 500 mA, yielding a voxel size of 0.12354325 mm. Part of the scan data were used in a previous study on the evolution of the sauropterygian labyrinth organ (Neenan et al., 2017).

Data processing. Using MIMICS Innovation Suite 24.0 (Materialise, Leuven, Belgium), the individual bones have been identified and traced throughout the µCT image stacks, generating a virtual 3D osteology. In SMNS 16363 the bones that could be identified and traced are the parietal, squamosals, pterygoids (plus associated bones dorsal to the pterygoids), basioccipital, supraoccipital, opisthotics, exoccipitals, prootics and parabasisphenoid (Fig. 3-6). Additionally, anatomical voids were virtually extracted and identified as representing nerves, vasculature and other original soft tissue correlates (Fig. 7-9). These include the cranial endocast, inner ear, sinus system, internal carotid arteries, and cranial nerves. The scan also revealed patches of dark, amorphous material, identified as plaster and artificial infilling, which is not easily identified externally in the specimen (Fig. 1; contrast enhanced in the 3D rendering shown in Supplementary Fig. 1). For the purposes of this study, the posterior-most portion of the braincase, from the upper temporal region backwards, has been segmented in detail. An overview of the entire cranium in lesser detail was segmented and visualised in VGStudio MAX 2024.1 (Volume Graphics, Heidelberg, Germany). The "Paint and Segment" tool, which utilises machine learning, was used to expedite the segmentation process. With the tool, discrete classes were assigned. Classes denote different types of material present within the scan, as characterised through different radiodensities (expressed in grey levels) and textures. The chosen classes for this scan were air, bone, matrix, and plaster. For every chosen class, a small part of the skull or otherwise representative material within the scan was segmented. The algorithm subsequently explores the rest of the volume, predicts which sections represent assigned classes,

and automatically segments these accordingly. Iterative improvements to correct for misclassification were manually implemented until satisfactory results were achieved. The 'create ROIs' (region of interest) tool was then used to create a 3D model of the cranium with the assigned classes as different regions of interest. The segmenting tools allowed the matrix between the teeth to be removed, after which the model was checked for any major inaccuracies. In addition, the parabasisphenoid and associated passages of the internal carotid arteries were also segmented in the entire skull scans of SMNS 16363 and GPIT/RE/09313; to reconstruct the complete antero-posterior extend of that bone within the crania (Fig. 2; Supplementary Fig. 2).

Results

Systematic Palaeontology

Sauropterygia Owen, 1860

Eosauropterygia Rieppel, 1994 [Rieppel, 1994a]

Nothosauroidea Nopcsa, 1928 [p. 172; not Baur, 1889]

Simosauridae Huene, 1948

Simosaurus gaillardoti Meyer, 1842

Osteological aspects

As in other sauropterygian reptiles (e.g., Edinger, 1921; Rieppel, 1994b, 2000; Allemand et al., 2023), the braincase of *Simosaurus gaillardoti* is formed by the basioccipital, supraoccipital, a pair of opisthotics, a pair of prootics, a pair of exoccipitals and the parabasisphenoid. These bones are bordered on the dorsal side by the parietal and squamosal forming the posterior skull roof and on the ventral side by the pterygoids (Fig. 3-6). Rieppel's (1994b) description of the braincase of *S. gaillardoti* presented the bones, foramina and other structures, which are used as a basis for the current study.

In SMNS 16363, the basioccipital, together with the exoccipitals, forms the ventral and ventrolateral borders of the foramen magnum. The basioccipital can be divided into two parts; the occipital condyle that protrudes straight posteriorly from the cranium on the posterior side and the internal bone that rests on the pterygoid at the posterior border of the cranium Fig. 5). It delimits the cranial endocast ventrally and supports the exoccipitals that project dorsolaterally from the basioccipital. Anteriorly, there is a clear gap separating the basioccipital from the

parabasisphenoid, although an in vivo cartilaginous connection cannot be ruled out. The exoccipitals extend between the basioccipital and the supraoccipital, form the ventrolateral borders of the foramen magnum, and are laterally flanked by the opisthotics. The exoccipitals participate in the occipital condyle dorsolaterally, but they are mostly separated from each other by the basioccipital. Each exoccipital bone is pierced by one foramen: the jugular foramen (Fig. 3), also called the metotic foramen (sensu Rieppel, 1994b). Laterally, the exoccipitals connect with the opisthotics.

The sutures between these bones are difficult to trace on the surface and in the scan data of SMNS 16363, so a small lateral connection between the opisthotics and the lateral portion of the basioccipital cannot be excluded.

The supraoccipital defines the dorsal border of the foramen magnum and its smooth, concave ventral surface saddles the endocast. It has a medial crest with lateral extensions flanking it on both sides. Anteriorly, this supraoccipital crest bifurcates, creating a Y-shape in dorsal view (Fig. 5A). The lateral surface is very irregular and the left and right side are not completely symmetrical in shape (Fig. 5C, D). The opisthotics connect with the exoccipitals and the supraoccipital and rest on the pterygoid laterally. On the dorsal and posterolateral side, the opisthotic meets the squamosal (Fig. 3), and the posttemporal fenestra perforates the suture between these two bones. The opisthotic meets the prootic on a small plane further anterior in the skull, which is visible only in lateral view (Fig. 5E, F). The fenestra ovalis (= fenestra vestibuli) is formed between the opisthotic and the prootic. No structure was found in SMNS 16363 that would indicate a stapes articulating with the fenestra ovalis. The prootic meets the supraoccipital dorsolaterally, but it is not visible in posterior view as it is obscured by the opisthotic, supraoccipital, and exoccipital in SMNS 16363. The prootic is a round-shaped element with a spongy internal bone structure that houses part of the vestibular system. The prootic meets the parietal dorsally, the supraoccipital posterodorsally, the opisthotic posteroventrally and it has an anterior inferior process that meets the parabasisphenoid ventromedially. The anterior border of the prootic frames the oval opening for the trigeminal cranial nerve (CN V) ventrally, posteriorly and dorsally (Fig. 5E; the anterior border of the opening remains free as there is no ossified laterosphenoid in SMNS 16363). The parabasisphenoid consists of two sections: the posterior section includes the sella turcica, posteriorly bounded by a low dorsum sellae, and the anterior

section forms wing-like lateral projections and a narrow medial process that projects anteriorly (Fig. 2, 5, 6). The sella turcica (Fig. 5A) is a saddle-shaped structure of the basisphenoid on the ventral side of the cranium, framed by bilateral (antero)dorsal extensions that are identified as the parabasisphenoid clinoid processes. As noted already for other *Simosaurus* specimens in Rieppel (1994), the sella turcica does not show a median dorsal ridge in the specimens studied herein. Due to damage and subsequent plastering of the pterygoids in SMNS 16363, the anterior extension of the parabasisphenoid and its relationship with the pterygoid is locally difficult to interpret. The wing-like lateral expansions and the medial process, expanding into a median septum anteriorly, form two distinctive anteroposteriorly trending trough-like structures (the cavum epiptericum described for *Nothosaurus* and *Simosaurus* by Rieppel, 1994b). Two prominent channels traverse the posterior portion of the parabasisphenoid that house the carotid arteries (see below). In GPIT/RE/09313, the parabasisphenoid and arrangement of the carotid passages was found to have overall the same shape as in the SMNS specimen, although in the former, the median septum and the clinoid processes are slightly more anteriorly expanded and inclined (hook-shaped; Supplementary Fig. 2). Slightly more anteriorly inclined clinoid processes are also visible in SMNS 10360 (Rieppel, 1994: fig. 6). In both our CT scans, the median septum shows a slightly concave posterior margin, a flat and narrow dorsal top, and an excavated anterior margin. A Y-shaped structure of the median septum in cross section as described by Rieppel (1994b: p. 14) could not be observed as both septa were laterally constricted in our studied specimens. The troughs lateral to the median septum are well marked only until the anterior border of the median septum and then taper anteriorly into a cultriform process which extends anteriorly to the level of the external nares. The cultriform process (Fig. 2; Supplementary Fig. 2) is laterally crested so the dorsal surface is concave (forming a wide dorsal groove along the process). Grooved and tapering cultriform processes were also described by a wide range of taxa, including for example the neodiapsid *Youngina capensis* (Gardner et al., 2010), the sauropodomorph dinosaur *Massospondylus carinatus* (Chapelle & Joiniere, 2018), and the millerettid *Milleropsis pricei* (Jenkins et al., 2025). In those taxa, the cultriform process does not reach the level of the external nares as is the case in *Simosaurus.* Towards its tip, the cultriform process seems to bifurcate slightly, which could be due to taphonomic processes. A similar bifurcation was observed in GPIT/RE/09313, but in this specimen the whole anterior palatal region split medially due to taphonomic distortion of the cranium.

The parietal is an unpaired and medially placed bone (Fig. 3) of the skull roof and it encloses the cranial endocast dorsally and dorsolaterally. The parietal foramen is well-defined, being medially positioned in the posterior skull table (posterior to the widest mediolateral expansion of the upper temporal fenestrae).

The suture between the parietal and the squamosal is partially obliterated externally as well as internally, rendering delimited segmentation of these elements impossible (Fig. 4). The posttemporal fenestra, between the squamosal and the opisthotic, leads to the fenestra ovalis (Fig. 5). The pterygoids form the palate in the braincase region (Fig. 6). Breaks in the pterygoid are filled with plaster mostly on the ventral side (Fig. 6B) thus obscuring large parts of the medial suture between the right and left pterygoid (Fig. 4, 6). Thus, the two pterygoids have been segmented as a single unit. . The pterygoid is a relatively flat bone in ventral view, forming a sturdy posteriorly extending quadrate ramus along which the quadrate is sutured laterally (note that the quadrate is not separately segmented herein because only a small portion was visible in the scan data of the higher resolution scan of the braincase region of SMNS 16363). In dorsal view, a thin u-shaped groove extends in posterolateral-anteromedial direction over the pterygoid surface, which anteriorly gets covered by a thin hook-shaped bone with a broad and narrow ventral base. Extending along both sides of the endocast and extending anterodorsally, these bones are interpreted as epipterygoids (Fig. 3, 4, 6), which in contrast to *Nothosaurus* do not contact the parietal dorsally (Rieppel, 1994b). . Within the pterygoid on the posterior side, the foramen for the internal carotid resides (see below). Between the pterygoid and the basioccipital large excavations exist that taper anteriorly (i.e, the paracondylar interstices; Fig. 3F).

Cranial endocast

Only the posterior portion of the cranial endocast of SMNS 16363, up to the level of the median septum of the parabasisphenoid was segmented out (Fig. 3, 7, 8).

Here, the endocranial void is delimited mostly by the dorsal, lateral and ~~and~~ ventral braincase elements. Anteriorly the endocast is not delimited laterally by bone. As such, the lateral edges of the endocast (Fig. 7, 8) are interpolated straight lines between the lowest point on any dorsal bone and the highest point on any ventral bone (Voeten et al. 2018). The endocast is wider dorsally than ventrally, granting it an oblong shape in both posterior and anterior view (Fig. 8). Posterodorsally, the endocast portion is delimited by the supraoccipital, posterolaterally by the

exoccipitals and opisthotics, posteroventrally by the basioccipital, ventrally by the parabasisphenoid, laterally by the prootics (and by the hook-like epipterygoids), and dorsally/dorsolaterally by the parietal. The endocast smoothly transitions into the sinus system posterodorsally (Fig. 8A, D), which renders delimitation of the cerebral endocast and adjacent sinusal structures locally challenging. The part of the endocast that is delimited by the parietal foramen projects vertically~~.~~

~~projects vertically,~~ where it expands slightly in diameter, and is dorsal portion is slightly offset to the left in SMNS 16363. The endocast is vaulted and relatively smooth posterior to the parietal foramen (which might have housed a pineal/parapineal gland; see Smith et al., 2018) and narrows posteriorly. Anterior to the level of the parietal foramen, the cerebral region of the endocast is present but not well defined laterally. On the posteroventral side, the endocast is delimited by the basioccipital, which defines a median groove with two flanking lobes. Anterior to this, the endocast is artificially smoothed during segmentation due to the absence of any ventral constriction. Here, the ventral boundary was interpolated between the basioccipital and the sella turcica. The sella turcica (Fig. 5A) forms an irregular relief on the endocast. Anterior to the sella turcica, the endocast is constricted by plaster and the pterygoid, which produce a bumpy relief until the ventral groove formed by the median septum of the parabasisphenoid is expressed. The internal carotids enter into the cranial endocast ventrally, and only a few of the posterior brain nerves could be traced to exit the endocast laterally (see below).

Nerves and blood vessels

The internal carotid arteries enter the cranium through the internal carotid foramen on the quadrate ramus of the pterygoid (Fig. 7, 8). The internal carotids then extend along the pterygoid dorsally and ventral to the parabasisphenoid (Fig. 6F). Distinct ridges are visible on the ventral side of the parabasisphenoid tracing the course of the internal carotid arteries. On the level of the clinoid processes of the parabasisphenoid, the carotid arteries bifurcate (Fig. 7A, B). The medial branches are the cerebral carotids, which exist the parabasisphenoid dorsally through two carotid foramina and then merge with the cranial endocast where they cannot be followed anymore. The lateral branches are the palatine arteries. Both palatine arteries can be followed for a short distance more anteriorly, after which they cannot be traced further. The two ventral lobes of the posteroventral endocast (Fig. 8C, D) which are expressed as two anteroposteriorly elongate

depressions in the basioccipital (Fig. 5H) likely housed paired basilar arteries that enter here into the endocast. Similar paired basilar arteries were discussed for the mosasaur *Platecarpus* (Russell, 1967) and have been segmented out also in braincase of *Plioplatecarpus peckensis* (Cuthbertson et al., 2015). The tubular groove (that partly could be roofed over) extending postolaterally-anterormedially over the pterygoid wings is interpreted to potentially have housed the lateral head vein (=vena capitis lateralis; see Russell, 1967).

A complex neurovascular system pervades the pterygoid as could be identified on the left side in SMNS 16363 (Fig. 3, 7, 8). Posteriorly on the ventral surface of the pterygoid, a foramen is present, identified as the likely entry of an artery into the pterygoid, but also potentially housing parts of the palatal branch of the facial cranial nerve (CN VII). This passage within the pterygoid extends as a larger canal that courses anteriorly, parallel to the internal carotid arteries. Smaller branches split off this canal, departing the pterygoid through a number of smaller foramina, three of which open onto the pterygoid dorsally and one foramen on the ventral side. The main canal extends further anteriorly and is visible through the foramen of the CN VII. Slightly posterior to the facial foramen, the canal splits into a complex branching system (leading to the aforementioned smaller foramina), which extends more laterally. At the level of the parietal foramen, the canal exits through the foramen for the presumed palatine branch of CN VII. A similar canal network was likely present also in the right pterygoid as evidenced by few small foramina on the dorsal bone surface, but it is only partially preserved due to the breakage of bone and reconstruction with plaster.

The jugular foramen is a structure that opens into the endocast and likely accommodated the cranial nerves IX-XII in SMNS 16363 (Fig. 3F, 7). The posteroventral portion likely accommodated CN XII and the more dorsal part for the passage of CN IX-XI (Fig. 8B, C). Another structure oblique to the semicircular canals of the inner ear would have connected with the cranial endocast, likely housing the vestibulocochlear nerve (CN VIII).

Other soft tissue structures

Connected to the endocast on the posterior-dorsal part is a large system of cavities (Fig. 8) pertaining to the cranial sinus system (Witmer et al., 2008; Dufeau & Witmer, 2015; Voeten et al., 2018). It can be followed from the connection to the endocast posteriorly between the skull roof bones (i.e., the parietal and squamosals) and the prootic. It then crosses over into the cavity

connected to the posttemporal fenestra between the opisthotic and parietal-squamosal. Within the opisthotics, prootics and supraoccipital, the endosseous labyrinth can only be partially reconstructed in SMNS 16363 (Fig. 7-9). The main body of the labyrinth, the vestibule, is oval-shaped. Most of the posterior semicircular canal (SC) could be reconstructed, meeting the anterior SC in the crus commune, whose ventral connection with the vestibule could not be completely reconstructed (Fig. 8E, 9A-D). Of the lateral and anterior SC, only the posterior (opisthotic) portions were traceable, whereas the canals could not be traced much further after entering the prootic. As reconstructed, the right and left labyrinth portions in SMNS 16363 generally agree with the morphology seen in the labyrinth extracted from GPIT/RE/09313 (Neenan et al., 2017: p. 3853).

Discussion

Osteological aspects

Much of Rieppel's (1994b) original identification of braincase morphology and interpretations of associated soft tissues can be confirmed by the present study of SMNS 16363 and GPIT/RE/09313. The usage of CT scan data of less or unprepared specimens, however, allowed for the identification and re-interpretation of some cranial structures related to the braincase region.

One of the surprising finds was the identification of clear epipterygoids in SMNS 16363 (Fig. 3, 4, 6, 9E-J). In contrast to Rieppel (1994b) stating the seeming absence of epipterygoids in *Simosaurus* (based mainly on acid-prepared specimens such as SMNS 10360, 50714 and 50715), two hook-shaped epipterygoids could be identified, whereas their absence in other specimens seems to be thus a preparatory (or preservational) artefact. The left epipterygoid bone has a small perforation in its triangular ventral portion (i.e. the pterygoid facet of the bone; Fig. 3C, 6D, E). However, this hole represents an artifact associated with a mechanical fracture (see Fig. 4B) rather than an original anatomical feature. In ~~GPIT~~ GPIT/RE/09313, the area where the epipterygoids would have been placed, is clearly damaged (Supplementary Fig. 2), as is the region in SMNS 10360 and SMNS 16767. The epipterygoids in SMNS 16363 lack a parietal contact and flank the anterior extend of the posterior ossified part of the parabasisphenoid complex. The latter expands into a median septum as indicated by Rieppel (1994b). The anatomical location of the median septum agrees with the ventral-dorsal extension of the

parabasisphenoid in SMNS 16363 anterior to the level of the parietal foramen, but a dorsal expansion (into a Y-shaped structure) was not observed in both CT-scanned specimens studied herein. Towards anterior, the parabasisphenoid extends as a tapering thin and grooved cultriform process up to the level of the external/internal nares. The process thus likely supported the infraorbital to rostral endocast (i.e., the olfactory tract) ventrally, as was shown also for *Nothosaurus marchicus* (Voeten et al., 2018).

The excavations lateral to the basioccipital have been referred to as eustachian foramen, as they were interpreted as housing the eustachian tube or the internal carotid arteries in *Nothosaurus* (Koken, 1893). As such, the eustachian tube was interpreted as connecting the middle ear and the pharyngeal region in these animals (Rieppel, 1994b). As shown by the previous study on *Nothosaurus marchicus* (Voeten et al., 2018), these excavations, termed paracondylar interstices in that study, did neither house the internal carotids, nor did they connect to the pharyngeal region (and thus not serving as a connection with the middle ear). In SMNS 16363, the paracondylar interstices (Fig. 3F) can be followed until the anterior end of the basioccipital, from where they do not connect to the endocast or the middle ear. As in *N. marchicus* (Voeten et al., 2018), any tiny spaces extending anteriorly to the paracondylar interstices are due to blunt abutting rather than a tight suturing of the braincase bones in this region.
In SMNS 16363, the medial pillars of the exoccipitals articulate more posteriorly and posterolaterally with the basioccipital, so that we here consider them to participate in the formation of the occipital condyle, in contrast to what has been reported for some other specimens of *Simosaurus gaillardoti* (Rieppel, 1994a, b).
As discussed by Rieppel (1994b), the location of the fenestra ovalis and structure of adjacent cranial elements are different between *Simosaurus* (SMNS 10360, 15860, 50714 and 50715) and *Nothosaurus* (SMNS 59075 and 59076). In *Simosaurus*, the fenestra ovalis is located between the opisthotic and prootic and is visible in lateral view, whereas the fenestra ovalis is not visible in lateral view in *Nothosaurus* (Rieppel, 1994b). Similar to Rieppel (1994b), no stapes was encountered in the studied specimens of *Simosaurus* herein.
The posttemporal fenestrae are arranged differently in *S. gaillardoti* compared to the reduced posttemporal foramen in *N. marchicus*, which in the latter are medial to the paracondylar Interstices (Voeten et al., 2018) but laterally placed in SMNS 16363. Voeten et al. (2018)

rejected the term ‘eustachian foramen’ (sensu Rieppel, 1994b; De Miguel Chaves et al., 2018a), rendering the placement and geometry of the paracondylar Interstices potentially more flexible, while arguing against the functions otherwise associated with an eustachian foramen.

The posttemporal fenestra (Fig. 3F) is located between the opisthotic and squamosal in *Simosaurus*, whereas the reduced posttemporal foramen in *Nothosaurus* is bordered by the exoccipital, supraoccipital and in some cases the opisthotic (e.g., Rieppel, 1994b; Voeten et al., 2018; Shang et al., 2022). In SMNS 16363, the posttemporal fenestrae are not as large as observed in *Placodus gigas* (Sues, 1987), but they are clearly visible and well-defined.

Placodonts were obligately durophagous, feeding primarily on hard-shelled prey (Rieppel, 2002). *S. gaillardoti* was also durophagous but likely supplemented its diet by catching fish using rapid snapping motions (Rieppel, 1994a). *N. marchicus*, in contrast, captured fish through a quick side-swipe motion with its distinct fish-trap dentition (Rieppel, 2000). This morphofunctional gradient coincides with a shift from large and well-defined posttemporal fenestrae in basal Triassic Sauropterygia to reduced or absent posttemporal foramina in nothosauroids. Progressive reduction of posttemporal fenestrae/foramina thus appears complementary to the development or enlarged upper temporal fenestrae in nothosauroids (Rieppel, 1994b) relative to placodonts, which are the sister taxon to Eosauropterygia. Continued specialisation and the establishment of obligate piscivory with clear fish-trap dentition in nothosaurids may explain the difference between the size of posttemporal fenestrae/foramina in *Simosaurus* and *Nothosaurus*, respectively.

Cranial endocast

The general shape of the endocast of *S. gaillardoti* is similar to that of *Nothosaurus* (Fig. 10), being elongated and tapering anteriorly with an anteroposterior orientation (e.g., Edinger, 1921; Voeten et al., 2018). The endocast of *P. gigas* is also elongated (Fig. 10C, D), but the shape is anteroposteriorly sigmoidal (Neenan & Scheyer, 2012). The most striking difference between the endocasts of *S. gaillardoti* (Fig. 10A, B) and *N. marchicus* (Fig. 10E, F) is the dorsoventral flatness of the latter (Voeten et al., 2018). The endocast of *S. gaillardoti* is narrower with a vertically oriented oval shape, whereas the endocast of *N. marchicus* has a more horizontally oriented oval shape. The flatness of the *N. marchicus* endocast can be attributed to its dorsoventrally flattened skull inferred to be hydrodynamically specialised for lurching ambush

predation (Voeten et al., 2018). The less flattened endocast of SMNS 16363 is thus likely associated with its less dorsoventrally flattened skull (which also might reflect a requirement for more robusticity/rigidity in a cranium that engages in facultative durophagy), indicating a more broad-spectrum feeding strategy that included both durophagy and piscivory (Rieppel, 1994a). The endocast of *S. gaillardoti* was also compared with the endocast of *Libonectes morgani* (Allemand et al., 2019). *L. morgani* is an elasmosaurid with an anteroposteriorly elongated endocast (Fig. 10d). Unlike *S. gaillardoti* and *N. marchicus*, the endocast of *L. morgani* (Fig. 10G, H) is dorsoventrally thick and distinctly thins at the anteroposterior level of the para-/pineal complex. Similarly, the endocast of *Dolichorhynchops* sp. would be posteriorly thickened based on the reconstructed braincase by Sato et al. (2011), although its anterior endocast portion remains elusive due to the lack of preserved bone in ROM 29010. The endocast of *L. morgani* also shows two well-defined lobes on the dorsal side posterior to the parapineal/pineal complex (Fig. 10G, H). The posterior lobe was interpreted to represent the cerebellum, and the anterior lobe associated with the optic lobe (Allemand et al., 2019; 2023). The endocast of *S. gaillardoti* shows a singular lobe posterior to the pineal complex (Fig. 10A), partly segmented as the sinus system. Extrapolating from the condition of *L. morgani*, this lobe could be either the cerebellum or the optic lobe. The optic lobes are placed more laterally in *N. marchicus*, which would suggest the referred lobe is the cerebellum in SMNS 16363. However, the cerebellum is often unpronounced in marine reptiles, and here even less developed than in plesiosaurs (Allemand et al., 2019). Thus, whether this lobe is the optic lobe, or the cerebellum remains unclear. The boundary between the pons (posterior-most midbrain) and the medulla oblongata (anterior-most hindbrain) could be recognised in *N. marchicus* based on a faint flexure (Fig. 10F) (Voeten et al., 2018). In *S. gaillardoti*, the endocast has a relatively consistent shape at the posterior-most portion, then expands laterally at the anterior end of the basioccipital And this could be the border of the medulla oblongata (Fig. 10A). It must be noted that the ventral border between the basioccipital and the parabasisphenoid is not well delimited due to a gap between both bones (which may have featured a cartilaginous connection during life; Fig. 6, 7). The boundary between pons and medulla oblongata border could thus also be placed more anteriorly in this transitional region.

Nerves and blood vessels

The internal carotid artery enters the skull through the jugular foramen which is more dorsally and medially placed in *S. gaillardoti* than in *N. marchicus*. The internal carotid arteries also split more anteriorly in *S. gaillardoti* than in *N. marchicus* and in plesiosaurs, . In the latter, they split even more anteriorly than in *S. gaillardoti*, specifically anterior to the basisphenoid (Allemand et al., 2023). The palatine nerve may have been housed by the branch containing the palatine artery in *S. gaillardoti*, which is the lateral branch after the bifurcation (Rieppel, 1994b).

Similar to the condition in *Nothosaurus* spp. (Rieppel, 1994b; Voeten et al., 2018) only the para- and basisphenoid complex region is ossified and fused in *Simosaurus gaillardoti*, whereas the more lateral/dorsal sphenoid regions remain un-ossified (i.e., a laterosphenoid is absent). As such, the cranial nerves I-IV can also not be reconstructed using the CT scanned specimens of *Simosaurus* and only a portion of the CN V is framed by the prootic creating only a partial prootic 'fenestra'. Although Neenan and Scheyer (2012) also indicated the absence of a laterosphenoid in *Placodus gigas*, a complete prootic fenestra is shown, surrounded by the bone of the prootic. Alternatively, the anterior and anterodorsal part of the fenestra might not be constructed by the prootic but by a thin laterosphenoid instead. A similar condition was, for example, also described in the early branching archosauromorph *Tanystropheus hydroides* (Spiekman et al., 2020). The laterosphenoid is generally considered a typical structure found in taxa of the archosaur lineage including extant crocodylians and birds (e.g., Kuzim et al. 2021), although Rieppel (1976) argued for referral of the bone in archosaurs as pleurosphenoid instead. In the latter study, the laterosphenoid of snakes was considered to be a non-homologous structure to that of archosaurs, based on differences in cranial development. The term laterosphenoid seemed to have gained traction in archosaur research, however, and a morphologically similar bone to that in the archosaur cranium has been proposed as a homologous element in the cranium of the stem turtle *Proganochelys quenstedtii* as well (Bhullar & Bever, 2009). Evers et al. (2019), however, argued that the fenestra prootica could not be considered a homologous structure to the trigeminal foramen, a secondarily formed structure in 'anatomically modern turtles' (Scheyer et al., 2022), further raising questions of homology of this part of the reptilian braincase feature, but a review of this feature would go beyond the scope of this article.

Rieppel (1994b) hypothesised that the palatine branch of the facial nerve could have emerged from the facial foramen and entered the foramen for the palatine branch of the facial nerve (VIIpl). The course of the facial nerve is unclear in our observed specimen, but this solution

seems unlikely considering the presence of the canal within the pterygoid between the facial foramen and VIIpl, as well as the presence of the canal more posteriorly than the facial foramen. According to Rieppel (1994b), each exoccipital in *S. gaillardoti* would carry two foramina, a larger anterior and a smaller posterior foramen, that house the hypoglossal nerve (CN XII). The specimen SMNS 16363 studied here in detail only shows one opening that corresponds with the jugular foramen, which is also called the metotic foramen in Rieppel (1994b). According to the scan data, we hypothesise that the single jugular foramen in SMNS 16363 corresponds to a combined hypoglossal and metotic foramen.

According to Rieppel (1994b), the foramen piercing the prootic ventral to the fenestra ovalis could have housed the hyomandibular branch of the facial nerve (VIIhy). The prootic in SMNS 16363 is porous and features a large foramen that correlates with Rieppel's (1994b) observations. Of the cranial nerves exiting the posterior portion of the brain, the glossopharyngeal (CN IX) and vagus (CN X) cranial nerves are intimately related and have been interpreted to enter through the jugular foramen in *N. marchicus* (Voeten et al. 2018). It seems possible that these nerves, together with the hypoglossal (CN XII) nerve (and the spinal accessory nerve CN XI) passed through the jugular foramen in *S. gaillardoti*. This condition would differ from *P. gigas*, in which these nerves do not enter through the same foramen (Neenan & Scheyer, 2012). The hypoglossal (CN XII) nerve in *P. gigas* exits through a foramen in between the exoccipital and the basioccipital (potentially a derived condition in placodonts), and the glossopharyngeal (CN IX) and vagus (CN X) nerves pass through the jugular foramen. The location where the nerves enter the cranial endocast is different between *S. gaillardoti* and *N. marchicus*. The nerves exit more ventrally in *N. marchicus* than in *S. gaillardoti*. In *S. gaillardoti*, the nerves merge into the endocast from the foramen magnum. The course of the nerves can also be followed further anterior in *N. marchicus* (Voeten et al., 2018), where they merge with the endocast ventral to the foramen magnum.

Other soft tissue structures

The large dorsal system connected to the endocast is likely the sinus system or houses parts of the middle cerebral vein (Voeten et al., 2018). The structure has a similar placement in *N. marchicus* but has a smoother transition into the endocast in *S. gaillardoti* than in *N. marchicus*, where it emerges relatively perpendicularly to the endocast.

The inner ear has been shown to have adaptations to aquatic life, where the semicircular canals have decreased height and/or increased width (Georgi & Sipla, 2008). Neenan et al. (2017) showed that the inner ear altered with changes in locomotion in marine reptiles. The inner ear of *Placodus gigas* was distinctly larger than the inner ears of all other members of Sauropterygia, following also general shape changes with the transition from near-shore swimmers such as *Nothosaurus* spp. and *S. gaillardoti* to pelagic swimmers such as *Callawayasaurus colombiensis* and *Libonectes morgani*. The endosseous labyrinth of plesiosaurs was found distinctly more compact, showing anteroposterior shortening and thickening of the semicircular canals (Neenan et al., 2017). These adaptations align with the morphology of the endosseous labyrinths of an extant crocodile (*Crocodylus acutus*) and an extant sea turtle (*Lepidochelys olivacea*). The inner ears of the extinct near-shore swimmers resembled that of the crocodylian, whereas the pelagic swimmers look more similar to that of the extant sea turtle. The inner ear of SMNS 16363 (Fig. 8E) has a similar morphology to that of GPIT/RE/09313, the *Nothosaurus* sp. specimen (NME 16/4), and the *Augustasaurus hagdorni s*pecimen (FMNH PR 1974) used in Neenan et al. (2017) and thus reflects the adaptions for aquatic life in near-shore environments.

Palaeoecological implications

SMNS 16363 has a braincase morphology that is quite similar to that of *Nothosaurus marchicus* (specimen TW480000375). The two share similar locations of fenestra, such as the posttemporal fenestra, and overall attachments of bones, such as the placement of the exoccipitals, supraoccipital and opisthotics (Rieppel, 1994b). These conditions are markedly different in placodonts. Additionally, internal structures such as the (para-)pineal complex and the endocast have a broadly similar shape (Fig. 10). The morphology of the inner ear in nothosaurs and simosaurs share the adaptions for near-shore aquatic life as they both feature a smaller endosseous labyrinth than placodonts, but dorsoventrally more elongated semicircular canals compared to the pelagic plesiosaurs (Neenan et al., 2017). Based on these similarities, the present study supports a closer relationship of *Simosaurus* with other nothosaurs within Nothosauroidea. The near-vertical projection of the parapineal/pineal complex in *Simosaurus* relative to its subtly forward-slanting orientation in *Nothosaurus* (Voeten et al., 2018) could reflect a slightly different mode of cranial development to facilitate the more specialised derived cranial architecture in the latter. Nothosauria have been interpreted as piscivorous ambush predators

with fish-trap dentition (Rieppel 2002; Voeten et al., 2018), whereas *Simosaurus gaillardoti* has a more generic (opportunistic) feeding strategy, including facultative durophagy (Rieppel 2002). This is supported here by the dorsoventrally flattened endocast of *Nothosaurus marchicus* (TW480000375; Voeten et al., 2018) relative to the less dorsoventrally flattened endocast (and skull) of SMNS 16363. Durophagy is also seen in the near-shore Placodontiformes which is usually regarded as the most basal sauropterygian clade (Rieppel, 1999, 2000, 2002). Like nothosaurs, pistosaurs have been interpreted as piscivorous (Storrs, 1993). Thus, piscivory with clear fish-trap dentition is interpreted here to have developed multiple times independently in several sauropterygian clades.

Conclusions

The braincase of *S. gaillardoti* had only been described exteriorly, using acid-prepared skulls and only a limited number of 3D segmented braincases of other Sauropterygia exist. The virtually segmented braincase of SMNS 16363 (and that of the partly segmented GPIT/RE/09313) gives new valuable information not available previously for *Simosaurus gaillardoti*. This provides a better understanding of the internal morphology of the bones and soft tissue structures, such as cranial nerves and vasculature. It also indicates the existence of epipterygoids in *S. gaillardoti* not observed earlier in acid-prepared specimens. The inner ear of SMNS 16363 is comparable to that of other near-shore sauropterygians in overall shape, sharing the adaptations for aquatic life but shallower aquatic than the open-water plesiosaurs as was previously indicated (Neenan et al., 2017). The braincase anatomy and the brain endocast support a phylogenetic placement of *Simosaurus gaillardoti* close to other nothosauroids. Also, piscivory is the currently proposed feeding strategy for most nothosaurs and pistosaurs but not for *S. gaillardoti* and *Paludidraco multidentatus*. Thus, clear fish-trap dentition piscivory could be interpreted as independently derived in nothosaurs and pistosaurs. Future research on more related taxa, along with additional scans and segmented endocasts across the phylogeny will provide additional, valuable information about sauropterygian phylogenetic relationships and their evolutionary history.

Acknowledgements

Daniel Snitting and Sifra Bijl (Uppsala University) are thanked for technical support, especially with MIMICS and VGStudio MAX. Feiko Miedema (Paläontologisches Institut, Universität Zürich, PIMUZ) is thanked for discussing aspects of reptilian braincase morphology. Stephan

Spiekman (SMNS) is thanked for additional images of *Simosaurus* specimens. Access to specimens were kindly granted by Rainer Schoch (SMNS) and Ingmar Werneburg (GPIT), and the CT datasets were acquired by Tobias Reich (formerly PIMUZ). Thanks to Remí Allemand (MNHN, Muséum national d'Histoire naturelle, Paris, France) for providing images of the cranial endocast of *Libonectes*. We also thank the staff working at the AST-RX facility at MNHN Paris, that made the scanning of the *Simosaurus* specimens possible.

References

Agassiz L. 1833-45. *Recherches sur les Poissons Fossiles, Vol. I-V [XLIX+188; XII+646; VIII+422; XVI+318; XII+282]*. Neuchâtel: Imprimaire de Petitpierre.

Allemand R, Houssaye A, Bardet N, and Vincent P. 2019. Endocranial anatomy of plesiosaurians (Reptilia, Plesiosauria) from the Late Cretaceous (Turonian) of Goulmima (southern Morocco). *Journal of Vertebrate Paleontology*:e1595636 (1595611 pages) [doi: 1595610.1591080/02724634.02722019.01595636].

Allemand R, Moon BC, and Voeten DFAE. 2023. The paleoneurology of Ichthyopterygia and Sauropterygia: Diverse endocranial anatomies of secondarily aquatic diapsids. In: Dozo MT, Paulina-Carabajal A, Macrini TE, and Walsh S, eds. *Paleoneurology of Amniotes*. Cham: Springer, 29–77 [https://doi.org/10.1007/1978-1003-1031-13983-13983_13983].

Bhullar B-AS, and Bever GS. 2009. An archosaur-like laterosphenoid in early turtles (Reptilia: Pantestudines). *Breviora* 518:1-11.

Cabezuelo-Hernández A, De Miguel Chaves C, and Pérez-García A. 2024. Sauropterygian remains from the Middle Triassic of Araif El-Naqa as the first identification of Simosauridae (Eosauropterygia) in Egypt. *Geobios* 87:1-7 [doi: 10.1016/j.geobios.2024.1008.1015].

Chapelle KEJ, and Choiniere JN. 2018. A revised cranial description of *Massospondylus carinatus* Owen (Dinosauria: Sauropodomorpha) based on computed tomographic scans and a review of cranial characters for basal Sauropodomorpha. *PeerJ* 6:e4224 [doi: 10.7717/peerj.4224].

Cheng Y-N, Wu X-c, Sato T, and Shan H-y. 2016. *Dawazisaurus brevis*, a new eosauropterygian from the Middle Triassic of Yunnan, China. *Acta Geologica Sinica (English Edition)* 90:401-424.

688 Cuthbertson R, Maddin HC, Holmes R, and Anderson JS. 2015. The braincase and endosseous
689 labyrinth of *Plioplatecarpus peckensis* (Mosasauridae, Plioplatecarpinae), with functional
690 implications for locomotor behaviour. *The Anatomical Record* 298:1597-1611 [doi:
691 1510.1002/ar.23180].
692 Dalla Vecchia FM. 2008. First record of Simosaurus (Sauropterygia, Nothosauoidea) from the
693 Carnian (Late Triassic) of Italy. *Revista Italiana di Paleontologia e Stratigrafia* 114:273-
694 285.
695 de Miguel Chaves C, Ortega F, and Pérez-García A. 2018. Cranial variability of the European
696 Middle Triassic sauropterygian *Simosaurus gaillardoti*. *Acta Palaeontologica Polonica*
697 63:315-326 [doi: 310.4202/app.00471.02018].
698 de Miguel Chaves C, Ortega F, and Pérez-García A. 2018. New highly pachyostotic
699 nothosauroid interpreted as a filter-feeding Triassic marine reptile. *Biology Letters* 14:
700 20180130 [doi: 10.1098/rsbl.2018.0130].
701 de Miguel Chaves C, Serrano A, Ortega F, and Pérez-García A. 2020. Braincase and
702 endocranium of the placodont *Parahenodus atancensis* de Miguel Chaves, Ortega & Pérez-
703 García, 2018, a representative of the highly specialized clade Henodontidae. *Comptes*
704 *Rendus Palevol* 19:173-186 [doi: 110.5852/cr-palevol2020v5819a5810].
705 Drevermann F. 1933. Die Placodontier. 3. Das Skelett von *Placodus gigas* Agassiz im
706 Senckenberg-Museum. *Abhandlungen der Senckenbergischen Naturforschenden*
707 *Gesellschaft* 38:321-364.
708 Dufeau, DL, and Witmer, LM. 2015. Ontogeny of the middle-ear air-sinus system in *Alligator*
709 *mississippiensis* (Archosauria: Crocodylia). *PLoS ONE* 10(9):e0137060 [doi:
710 10.1371/journal.pone.0137060].
711 Edinger T. 1921. Über *Nothosaurus*. I. Ein Steinkern der Schädelhöhle. *Senckenbergiana* 3:121-
712 129.
713 Gardner NM, Holliday CM, and O'Keefe FR. 2010. The braincase of *Youngina capensis*
714 (Reptilia, Dipsida): new insights from high-resolution CT scanning of the holotype.
715 *Palaeontologia Electronica* Vol. 13, Issue 3; 19A:16p [http://palaeo-
716 electronica.org/2010_3/217/index.html].
717 Georgi JA, and Sipla JS. 2008. Comparative and functional anatomy of balance in aquatic
718 reptiles and birds. In: Thewissen JGM, and Nummela S, eds. *Sensory Evolution on the*

719 *Threshold Adaptations in Secondarily Aquatic Vertebrates [ISBN 978-0-520-25278-3]*.
720 Berkeley: University of California Press, 233-256.
721 Germain D, and Ladevèze S. 2021. Methodological Focus A. The New Scalpel: Basic Aspects of
722 CT-Scan Imaging. In: Buffrénil Vd, Ricqlès Ad, Zylberberg L, Padian K, Laurin M, and
723 Quilhac A, eds. *Vertebrate Skeletal Histology and Paleohistology*. Boca Raton: CRC Press,
724 55-58.
725 Huene FRv. 1948. *Simosaurus* and *Corosaurus*. *American Journal of Science* 246:41-43.
726 Jenkins XA, Benson RBJ, Ford DP, Browning C, Fernandez V, Griffiths E, Choiniere J, and
727 Peecook BR. 2025. Cranial osteology and neuroanatomy of the late Permian reptile
728 *Milleropsis pricei* and implications for early reptile evolution. *Royal Society Open Science*
729 12:241298 [doi: 10.1098/rsos.241298].
730 Jiang D-Y, Motani R, Hao W-C, Rieppel O, Sun Y-L, Schmitz L, and Sun Z-Y. 2008. First
731 record of Placodontoidea (Reptilia, Sauropterygia, Placodontia) from the Eastern Tethys.
732 *Journal of Vertebrate Paleontology* 28:904-908.
733 Jiang D-Y, Motani R, Tintori A, Rieppel O, Chen G-B, Huang J-D, Zhang R, Sun Z-Y, and Ji C.
734 2014. The Early Triassic eosauropterygian *Majiashanosaurus discocoracoidis*, gen. et sp.
735 nov. (Reptilia, Sauropterygia), from Chaohu, Anhui Province, People's Republic of China.
736 *Journal of Vertebrate Paleontology* 34:1044-1052 [doi:
737 1010.1080/02724634.02722014.02846264].
738 Kear B, Rich T, Vickers Rich PV, Ali MA, Al-Mufarrih YA, Matari AH, Al-Masary AM, and
739 Halawani MA. 2010. A review of aquatic vertebrate remains from the Middle–Upper
740 Triassic Jilh Formation of Saudi Arabia. *Proceedings of the Royal Society of Victoria*
741 122:1-8 [doi: 10.1071/RS10001].
742 Kear BP, Engelschiøn VS, Hammer Ø, Roberts AJ, and Hurum JH. 2023. Earliest Triassic
743 ichthyosaur fossils push back oceanic reptile origins. *Current Biology* 33:R178-R179 [doi:
744 110.1016/j.cub.2022.1012.1053].
745 Kear BP, Roberts AJ, Young G, Terezow M, Mantle DJ, Santos Barros I, and Hurum JH. 2024.
746 Oldest southern sauropterygian reveals early marine reptile globalization. *Current Biology*
747 34:R562-R563 [doi: 510.1016/j.cub.2024.1003.1035].

748 Klein N, and Griebeler EM. 2018. Growth patterns, sexual dimorphism, and maturation modeled
749 in Pachypleurosauria from Middle Triassic of central Europe (Diapsida: Sauropterygia).
750 *Fossil Record* 21:137-157 [doi: 110.5194/fr-5121-5137-2018].
751 Klein N. 2009. Skull morphology of *Anarosaurus heterodontus* (Reptilia: Sauropterygia:
752 Pachypleurosauria) from the lower Muschelkalk of the Germanic Basin (Winterswijk, the
753 Netherlands) *Journal of Vertebrate Paleontology* 29:665-676 [doi:
754 610.1671/1039.1029.0327].
755 Klein N. 2010. Long bone histology of Sauropterygia from the Lower Muschelkalk of the
756 Germanic Basin provides unexpected implications for phylogeny. *PLoS ONE* 5(7): e11613
757 [doi: 10.1371/journal.pone.0011613].
758 Klein N, Houssaye A, Neenan JM, and Scheyer TM. 2015. Long bone histology and
759 microanatomy of Placodontia (Diapsida: Sauropterygia). *Contributions to Zoology* 84:59-
760 84 [doi: 10.1163/18759866-08401005].
761 Klein N, Sander PM, Krahl A, Scheyer TM, and Houssaye A. 2016. Diverse aquatic adaptations
762 in *Nothosaurus* spp. (Sauropterygia)—inferences from humeral histology and
763 microanatomy. *PLoS ONE* 11(7):e0158448 [doi: 10.1371/journal.pone.0158448].
764 Klein N, Wintrich T, Hagdorn H, Spiller D, Winkelhorst H, Goris G, and Scheyer TM. 2022.
765 *Placodus* (Placodontia, Sauropterygia) dentaries from Winterswijk, The Netherlands
766 (middle Anisian) and Hünfeld, Hesse, Germany (late Anisian) with comments on
767 ontogenetic changes. *PalZ* 96:289-302 [doi: 210.1007/s12542-12022-00614-w].
768 Koken E. 1893. Beiträge zur Kenntnis der Gattung *Nothosaurus*. *Zeitschrift der Deutschen*
769 *Geologischen Gesellschaft* 45:337-377.
770 Kuzmin IT, Boitsova EA, Gombolevskiy VA, Mazur EV, Morozov SP, Sennikov AG, Skutschas
771 PP, and Sues H-D. 2021. Braincase anatomy of extant Crocodylia, with new insights into
772 the development and evolution of the neurocranium in crocodylomorphs. *Journal of*
773 *Anatomy* 239:983-1038 [doi: 1010.1111/joa.13490].
774 Laboury A, Scheyer TM, Klein N, Stubbs TL, and Fischer V. 2023. High phenotypic plasticity at
775 the dawn of the sauropterygian radiation. *PeerJ* 11:e15776 [doi: 10.7717/peerj.15776].
776 Leyhr, J. 2023. Musculoskeletal Development in Jawed Vertebrates: Gene function, cis-
777 regulation, and 3D phenotypes in zebrafish. (PhD Thesis). *Acta Universitatis Upsaliensis*
778 [https://www.diva-portal.org/smash/record.jsf?pid=diva2:1789545].

779 Li Q, and Liu J. 2020. An Early Triassic sauropterygian and associated fauna from South China
780 provide insights into Triassic ecosystem health. *Communications Biology* 3:63 [doi:
781 10.1038/s42003-020-0778-7].
782 Liao J-l, Lan T, Xu G-h, Li J, Qin Y-j, Zaho M-s, Li X-l, and Wang Y. 2021. Tooth structure and
783 replacement of the Triassic *Keichousaurus* (Sauropterygia, Reptilia) from South China.
784 *Frontiers in Ecology and Evolution* 9:741851 [doi: 10.3389/fevo.2021.741851].
785 Marquez-Aliaga A, Klein N, Reolid M, Plasencia P, Villena JA, and Martinez-Perez C. 2017. An
786 enigmatic marine reptile, *Hispaniasaurus cranioelongatus* (gen. et sp. nov.) with
787 nothosauroid affinities from the Ladinian of the Iberian Range (Spain). *Historical Biology*
788 31:223-233 [doi: 210.1080/08912963.08912017.01359264].
789 Meyer Hv. 1842. *Simosaurus*, die Stumpfschnauze, ein Saurier aus dem Muschelkalke von
790 Luneville. *Neues Jahrbuch für Mineralogie, Geognosie, Geologie und Petrefaktenkunde*
791 1842:184-198.
792 Miedema F, Spiekman SNF, Fernandez V, Reumer JWF, and Scheyer TM. 2020. Cranial
793 morphology of the tanystropheid *Macrocnemus bassanii* unveiled using synchrotron
794 microtomography. *Scientific Reports* 10: 12412 [doi: 10.1038/s41598-020-68912-4].
795 Neenan JM, and Scheyer TM. 2012. The braincase and inner ear of *Placodus gigas*
796 (Sauropterygia, Placodontia)—a new reconstruction based on micro-computed
797 tomographic data. *Journal of Vertebrate Paleontology* 32:1350-1357 [doi:
798 1310.1080/02724634.02722012.02695241].
799 Neenan JM, Klein N, and Scheyer TM. 2013. European origin of placodont marine reptiles and
800 the evolution of crushing dentition in Placodontia. *Nature Communications* 4:1621 [doi:
801 10.1038/ncomms2633].
802 Neenan JM, Li C, Rieppel O, and Scheyer TM. 2015. The cranial anatomy of Chinese placodonts
803 and the phylogeny of Placodontia (Diapsida: Sauropterygia). *Zoological Journal of the*
804 *Linnean Society* 175:415-428 [doi: 410.1111/zoj.12277].
805 Neenan JM, Reich T, Evers SW, Druckenmiller PS, Voeten DFAE, Choiniere JN, Barrett PM,
806 Pierce SE, and Benson RBJ. 2017. Evolution of the sauropterygian labyrinth with
807 increasingly pelagic lifestyles. *Current Biology* 27:3852-3858 [doi:
808 3810.1016/j.cub.2017.3810.3069].

809 Nopcsa FB. 1928. The genera of reptiles. *Geologica hungarica (Ser Palaeontologica), Budapest,*
810 *Fasc 1 (1928)* 1:163-188.
811 Nosotti S, and Rieppel O. 2002. The braincase of *Placodus* Agassiz, 1833 (Reptilia,
812 Placodontia). *Memorie della Società Italiana di Scienze Naturali e del Museo Civico di*
813 *Storia Naturale di Milano* 31:3-18.
814 Owen R. 1860. *Palaeontology, or, a systematic summary of extinct animals and their geological*
815 *relations*. Edinburgh: Adam and Charles Black.
816 Pommery Y, Scheyer TM, Neenan JM, Reich T, Fernandez V, Voeten DFAE, Losko AS, and
817 Werneburg I. 2021. Dentition and Feeding in Placodontia: tooth replacement in *Henodus*
818 *chelyops*. *BMC Ecology and Evolution* 21:136 [doi: 10.1186/s12862-021-01835-4].
819 Qiao Y, Liu J, Wolniewicz AS, Iijima M, Shen Y, Wintrich T, Li Q, and Sander PM. 2022. A
820 globally distributed durophagous marine reptile clade supports the rapid recovery of
821 pelagic ecosystems after the Permo-Triassic mass extinction. *Communications Biology* 5:
822 1242 [doi: 10.1038/s42003-022-04162-6].
823 Rieppel O. 1976. The homology of the laterosphenoid bone in snakes. *Herpetologica* 32:426-
824 429.
825 Rieppel O. 1994a. Osteology of *Simosaurus gaillardoti* and the relationships of stem-group
826 Sauropterygia. *Fieldiana (Geology), New Series* 28:1-85.
827 Rieppel O. 1994b. The braincases of *Simosaurus* and *Nothosaurus*: monophyly of the
828 Nothosauridae (Reptilia: Sauropterygia). *Journal of Vertebrate Paleontology* 14:9-23.
829 Rieppel O. 1995. The genus *Placodus*: systematics, morphology, paleobiogeography, and
830 paleobiology. *Fieldiana: Geology, New Series* 31:1-44.
831 Rieppel O. 1999. Phylogeny and paleobiogeography of Triassic Sauropterygia: problems solved
832 and unresolved. *Palaeogeography, Palaeoclimatology, Palaeoecology* 153:1-15.
833 Rieppel O. 2000. Sauropterygia I - Placodontia, Pachypleurosauria, Nothosauroidea,
834 Pistosauroidea. *Handbuch der Paläoherpetologie [Handbook of Paleoherpetology]* Part
835 12A:1-134.
836 Rieppel O. 2002. Feeding mechanics in Triassic stem-group sauropterygians: the anatomy of a
837 successful invasion of Mesozoic seas. *Zoological Journal of the Linnean Society* 135:33-
838 63.

Russell DA. 1967. Systematics and morphology of American mosasaurs. *Peabody Museum of Natural History Bulletin* No. 23:1-241.

Sato T, Wu X-C, Tirabasso A, and Bloskie P. 2011. Braincase of a polycotylid plesiosaur (Reptilia: Sauropterygia) from the Upper Cretaceous of Manitoba, Canada. *Journal of Vertebrate Paleontology* 31:313-329 [doi: 310.1080/02724634.02722011.02550358].

Scheyer TM, Romano C, Jenks J, and Bucher H. 2014. Early Triassic marine biotic recovery: the predators' perspective. *PLoS ONE* 9(3): e88987 [doi: 10.1371/journal.pone.0088987].

Scheyer TM, Neenan JM, Bodogan T, Furrer H, Obrist C, and Plamondon M. 2017. A new, exceptionally preserved juvenile specimen of *Eusaurosphargis dalsassoi* (Diapsida) and implications for Mesozoic marine diapsid phylogeny. *Scientific Reports* 7: 4406 [doi: 10.1038/s41598-017-04514-x].

Scheyer TM, Neuman AG, and Brinkman DB. 2019. A large marine eosauropterygian reptile with affinities to nothosauroid diapsids from the Early Triassic of British Columbia, Canada. *Acta Palaeontologica Polonica* 64:745-755 [doi: 710.4202/app.00599.02019].

Scheyer TM, Klein N, Evers SW, Mautner A-K, and Pabst B. 2022. First evidence of *Proganochelys quenstedtii* (Testudinata) from the *Plateosaurus* bonebeds (Norian, Late Triassic) of Frick, Canton Aargau, Switzerland. *Swiss Journal of Palaeontology* 141:17 [doi: 10.1186/s13358-022-00260-4].

Shang Q-H, Li C, and Wang W. 2022. *Nothosaurus luopingensis* n. sp. (Sauropterygia) from the Anisian, Middle Triassic of Luoping, Yunnan Province, China. *Vertebrata PalAsiatica* 60:249-270 [doi: 210.19615/j.cnki.12096-19899.220524].

Smith KT, Bhullar B-AS, Köhler G, and Habersetzer J. 2018. The only known jawed vertebrate with four eyes and the bauplan of the pineal complex. *Current Biology* 28 (7): P1101-1107.e2 [doi: 10.1016/j.cub.2018.02.021].

Storrs GW. 1993. Function and phylogeny in sauropterygian (Diapsida) evolution. *American Journal of Science* 293-A:63-90.

Sues H-D. 1987. On the skull of *Placodus gigas* and the relationships of the Placodontia. *Journal of Vertebrate Paleontology* 7:138-144 [http://www.jstor.org/stable/4523133].

Sutton M, Rahman I., and Garwood R. 2016. Virtual paleontology—an overview. *The Paleontological Society Papers 22*:1-20.

Sutton MD. 2008. Tomographic techniques for the study of exceptionally preserved fossils. *Proceedings of the Royal Society of London, B* 275:1587-1593 [doi:1510.1098/rspb.2008.0263].

Sutton MD, Rahman IA, and Garwood RJ. (eds.) 2014. Techniques for Virtual Palaeontology. New Analytical Methods in Earth and Environmental Science. Hoboken, New Jersey: Wiley Blackwell. p 200.

Voeten DFAE, Reich T, Araújo R, and Scheyer TM. 2018. Synchrotron microtomography of a *Nothosaurus marchicus* skull informs on nothosaurian physiology and neurosensory adaptations in early Sauropterygia. *PLoS ONE* 13(1): e0188509 [doi: 10.1371/journal.pone.0188509].

Voeten DFAE, Albers PCH, and Klein N. 2019. Nothosauroidea from the Vossenveld Formation and their relatives. *Grondboor & Hamer* Volume 73 nr 5/6 - 2019 - Edition Staringia 16:234-244.

Wang W, Shang Q, Cheng L, Wu X-C, and Li C. 2022. Ancestral body plan and adaptive radiation of sauropterygian marine reptiles. *iScience* 25(12):105635 [doi: 10.1016/j.isci.2022.105635].

Wintrich T, Hayashi S, Houssaye A, Nakajima Y, and Sander PM. 2017. A Triassic plesiosaurian skeleton and bone histology inform on evolution of a unique body plan. *Science Advances* 3: e1701144 [doi: 10.1126/sciadv.1701144].

Witmer LM, Ridgely RC, Dufeau DL, and Semones MC. 2008. Using CT to peer into the past: 3D visualization of the brain and ear regions of birds, crocodiles, and nonavian dinosaurs. In: Endo H, and Frey R, eds. *Anatomical Imaging Towards a New Morphology [ISBN: 978-4-431-76932-3; 105 pp]*. Tokyo: Springer, 67-87 [doi: 10.1007/978-4-431-76933-0_6].

Wolniewicz A, Shen Y, Li Q, Sun Y, Qiao Y, Chen Y, Hu Y-W, and Liu J. 2023. An armoured marine reptile from the Early Triassic of South China and its phylogenetic and evolutionary implications. *eLife* 12:e83163 [doi: 10.7554/eLife.83163].

Xing L, Klein H, Lockley MG, Wu X-C, Benton MJ, Zeng R, and Romilio A. 2020. Footprints of marine reptiles from the Middle Triassic (Anisian-Ladinian) Guanling Formation of Guizhou Province, southwestern China: The earliest evidence of synchronous style of

swimming. *Palaeogeography, Palaeoclimatology, Palaeoecology* 558: 109943 [doi: 10.1016/j.palaeo.2020.109943].

Figure 1

Figure 1: Phylogenetic framework of Sauropterygia and studied specimen.

(A) Hypothesis modified from Allemand et al. (2023 and references therein), reflecting the traditional topology of sauropterygians and *Simosaurus* as sister to other nothosaurs. (B) Hypothesis modified from Li and Liu (2020) in which *Simosaurus* was found being more highly nested within nothosaurs. (C) Hypothesis modified from Wang et al., (2022) showing *Simosaurus* as sister to the clade consisting of nothosaurs and pistosauroids. (D-F) Cranium of *Simosaurus gaillardoti* (SMNS 16363) in dorsal (D), ventral (E), and occipital (F) view. Abbreviations: Eo, Eosauropterygia; Eu, Eusauropterygia; No, Nothosauroidea; Pi, Pistosauroidea; Sa, Sauropterygia.

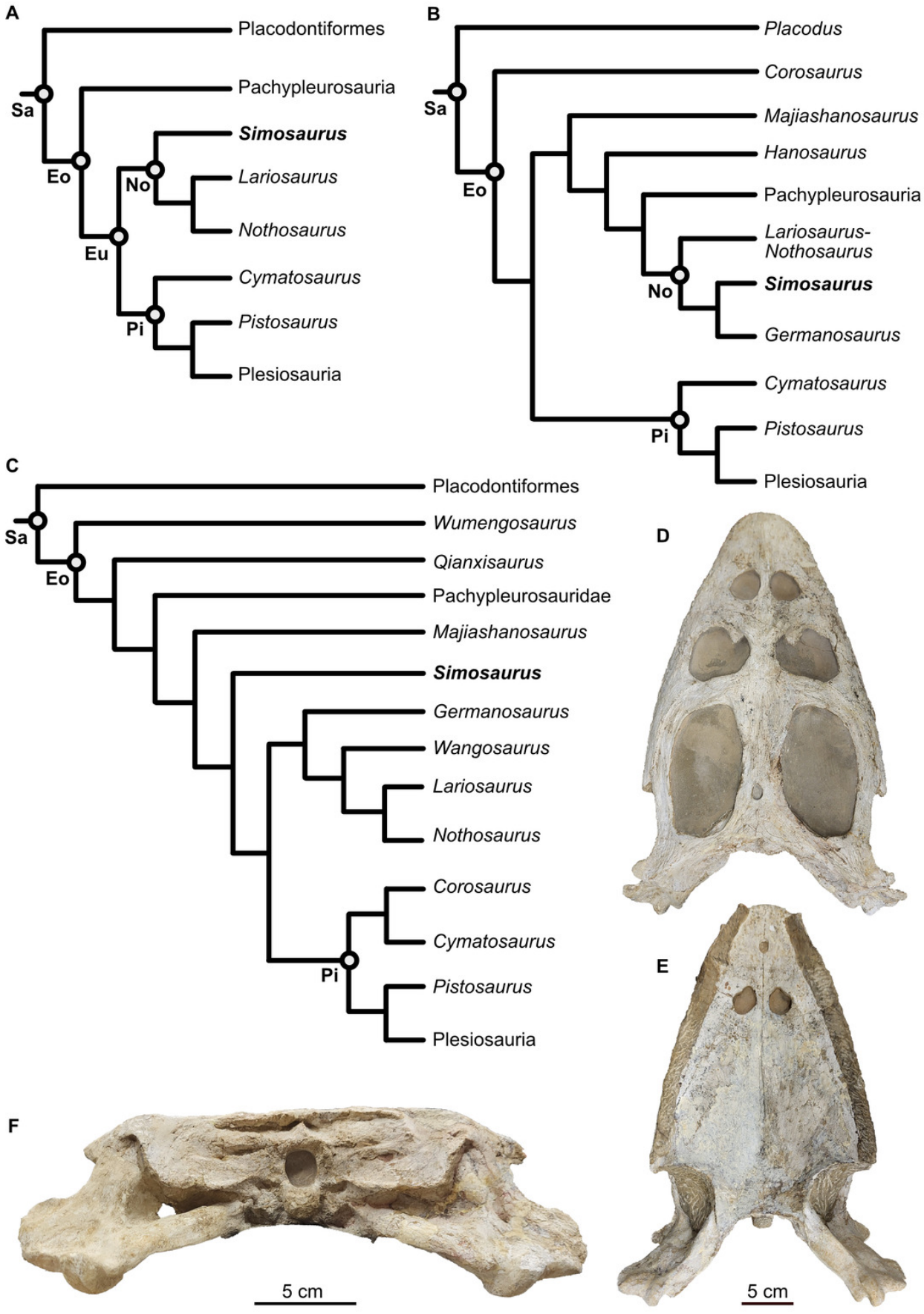
A
Placodontiformes
Pachypleurosauria
Simosaurus
Lariosaurus
Nothosaurus
Cymatosaurus
Pistosaurus
Plesiosauria
Sa
Eo
No
Eu
Pi
B
Placodus
Corosaurus
Majiashanosaurus
Hanosaurus
Pachypleurosauria
Lariosaurus-
Nothosaurus
Simosaurus
Germanosaurus
Cymatosaurus
Pistosaurus
Plesiosauria
Sa
Eo
No
Pi
C
Placodontiformes
Wumengosaurus
Qianxisaurus
Pachypleurosauridae
Majiashanosaurus
Simosaurus
Germanosaurus
Wangosaurus
Lariosaurus
Nothosaurus
Corosaurus
Cymatosaurus
Pistosaurus
Plesiosauria
Sa
Eo
Pi
D
E
F
5 cm
5 cm

Figure 2

Figure 2: Virtual rendering and partial segmentation of the full skull of *Simosaurus gaillardoti* (SMNS 16363).

(A-C) Partially transparent skull in showing the position and extent of the parabasisphenoid region, in dorsal (A), angled left anterolateral (B), and left lateral (C) view. (D-F) Segmented parabasisphenoid (in turquoise) and associated major blood vessels (in red), in left lateral (D), dorsal (E), and ventral (F) view. (G, H) Angled surface renderings of skull with virtual sections showing the anterior snout (G) and braincase (H) regions in coronal view. Elements not to scale.

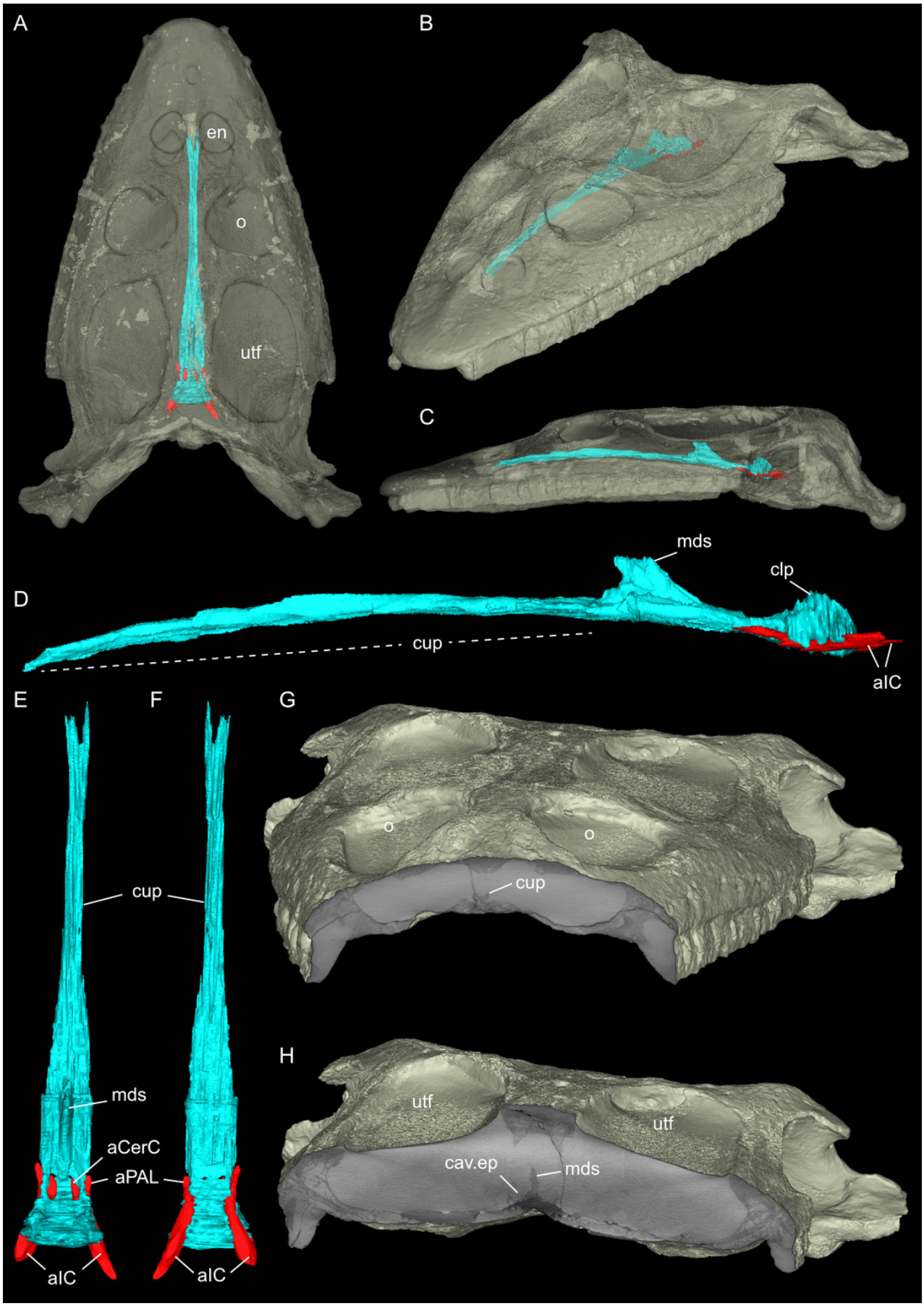
A
en
o
utf
B
C
mds
clp
D
cup
alC
E
F
G
cup
o
o
cup
mds
aCerC
aPAL
alC
alC
H
utf
utf
cav.ep
mds

Figure 3

Figure 3: Virtual rendering and segmentation of the full braincase region of *Simosaurus gaillardoti* (SMNS 16363).

Braincase region in dorsal (A), ventral (B), left lateral (C), right lateral with (D) and without cranial endocast and rendered blood vessels (E), and occipital view (F). Elements not to scale.

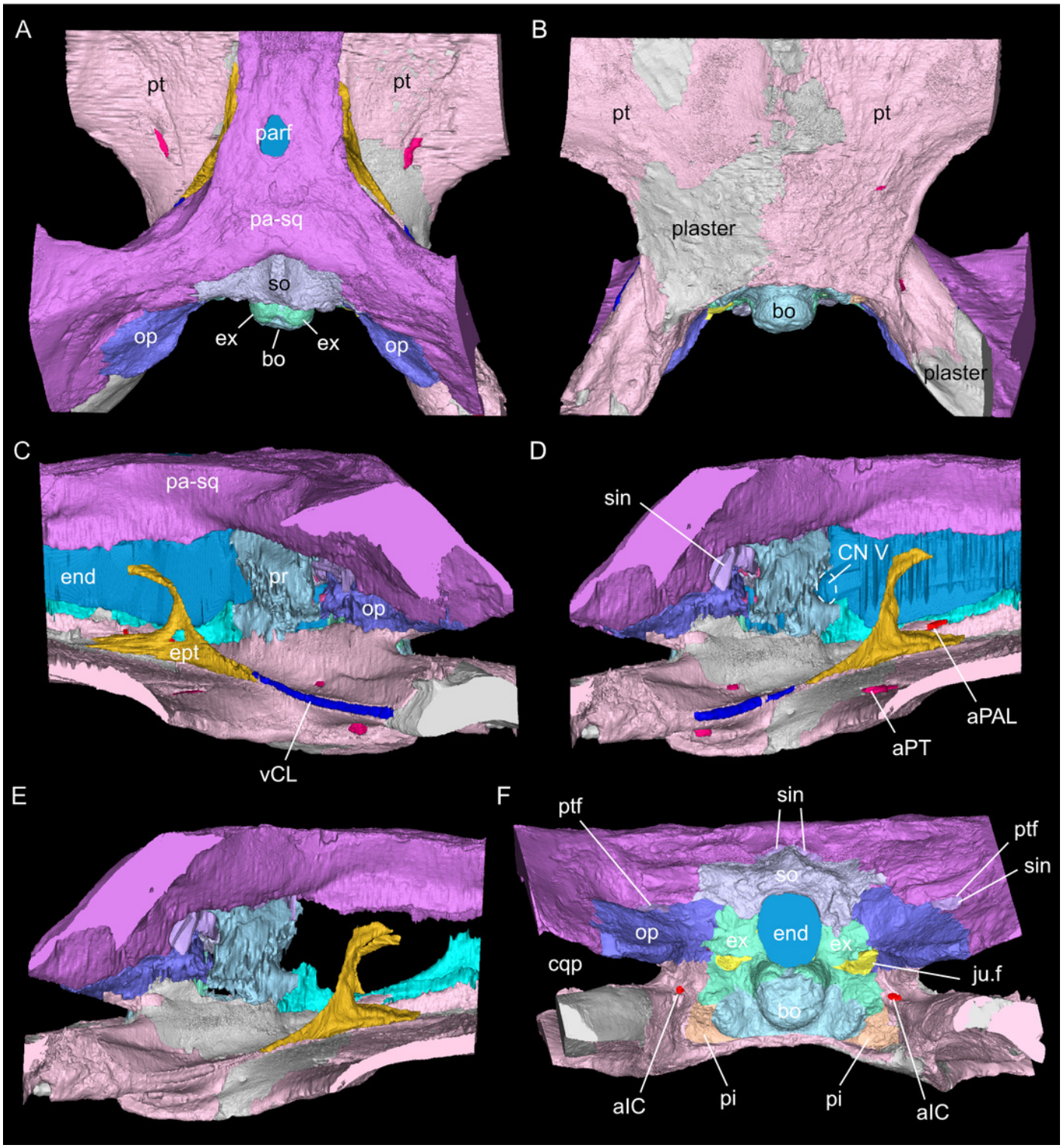
A
pt
pt
parf
pa-sq
so
op
ex
bo
ex
op
B
pt
pt
plaster
bo
plaster
C
pa-sq
end
pr
op
ept
vCL
D
sin
CN V
aPAL
aPT
E
F
ptf
sin
ptf
sin
so
op
ex
end
ex
cqp
ju.f
bo
aIC
pi
pi
aIC

Figure 4

Figure 4: Micro-CT slice data of *Simosaurus gaillardoti* (SMNS 16363).

(A) Coronal view of braincase region (A) indicating that the bone loss in the specimen occurred mainly due to the breakage of the specimen, as the filled in plaster closely follows the outlines of the preserved bones. (B) Coronal view through braincase at the level of the parietal foramen. The two epipterygoids are clearly visible in articulation with the underlying pterygoids. (C) Axial view of the skull roof bones. Note that the sutures between parietal and the squamosals are only partially visible, potentially indicating incipient fusion of the bones.

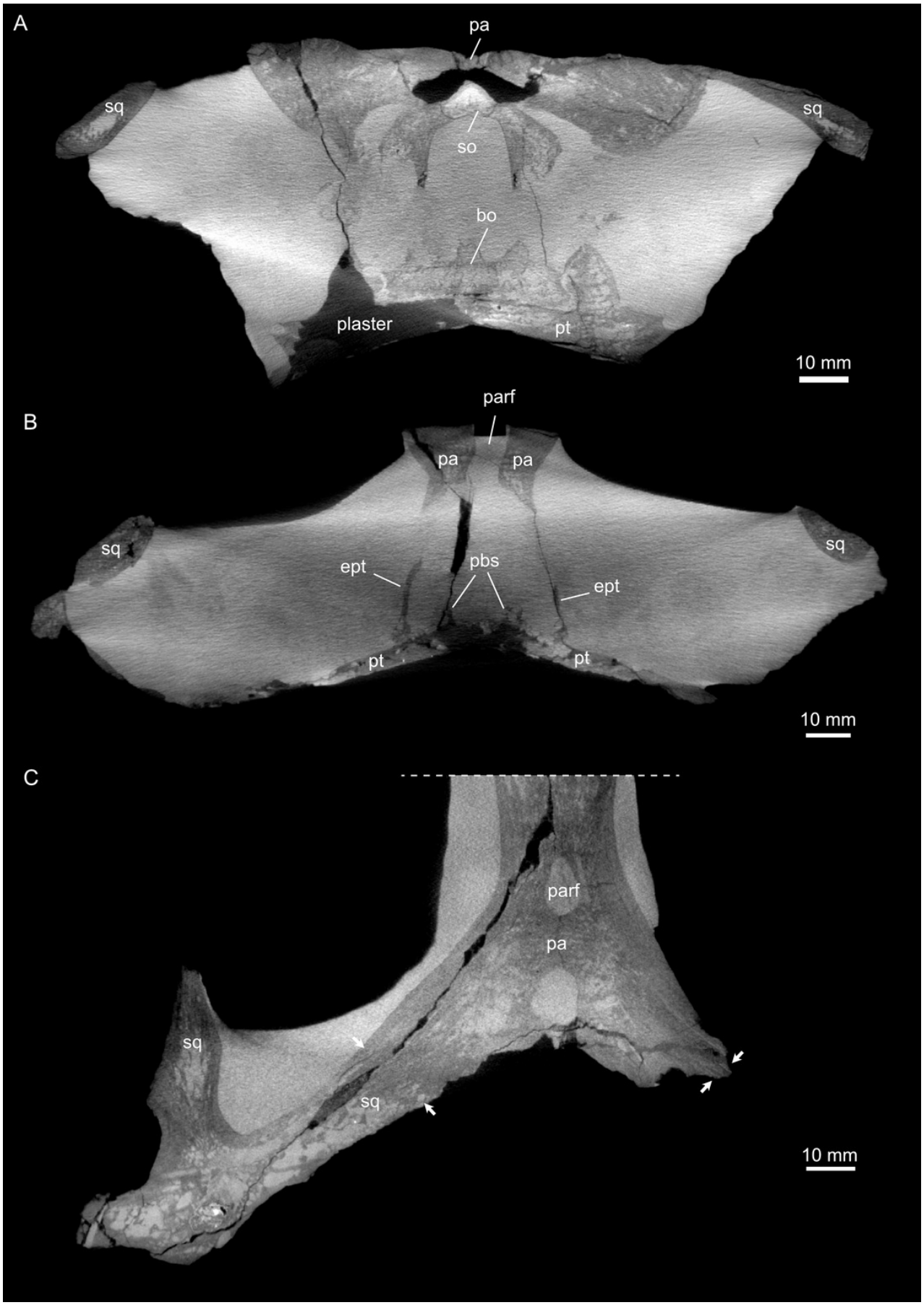
A
pa
sq
sq
so
bo
plaster
pt
10 mm
B
parf
pa
pa
sq
sq
ept
pbs
ept
pt
pt
10 mm
C
parf
pa
sq
sq
10 mm

Figure 5

Figure 5: Virtual rendering and segmentation of bony elements forming the braincase of *Simosaurus gaillardoti* (SMNS 16363).

Braincase in dorsal (A), ventral (B), occipital (C), rostral (D), left lateral (E), right lateral (F), angled right posterolateral (G), and angled left anterolateral view (H). Dashed lines in (E) and (F) indicate anterior delimitation of the parabasisphenoid in this higher resolution-, but spatially limited micro-CT scan. Elements not to scale.

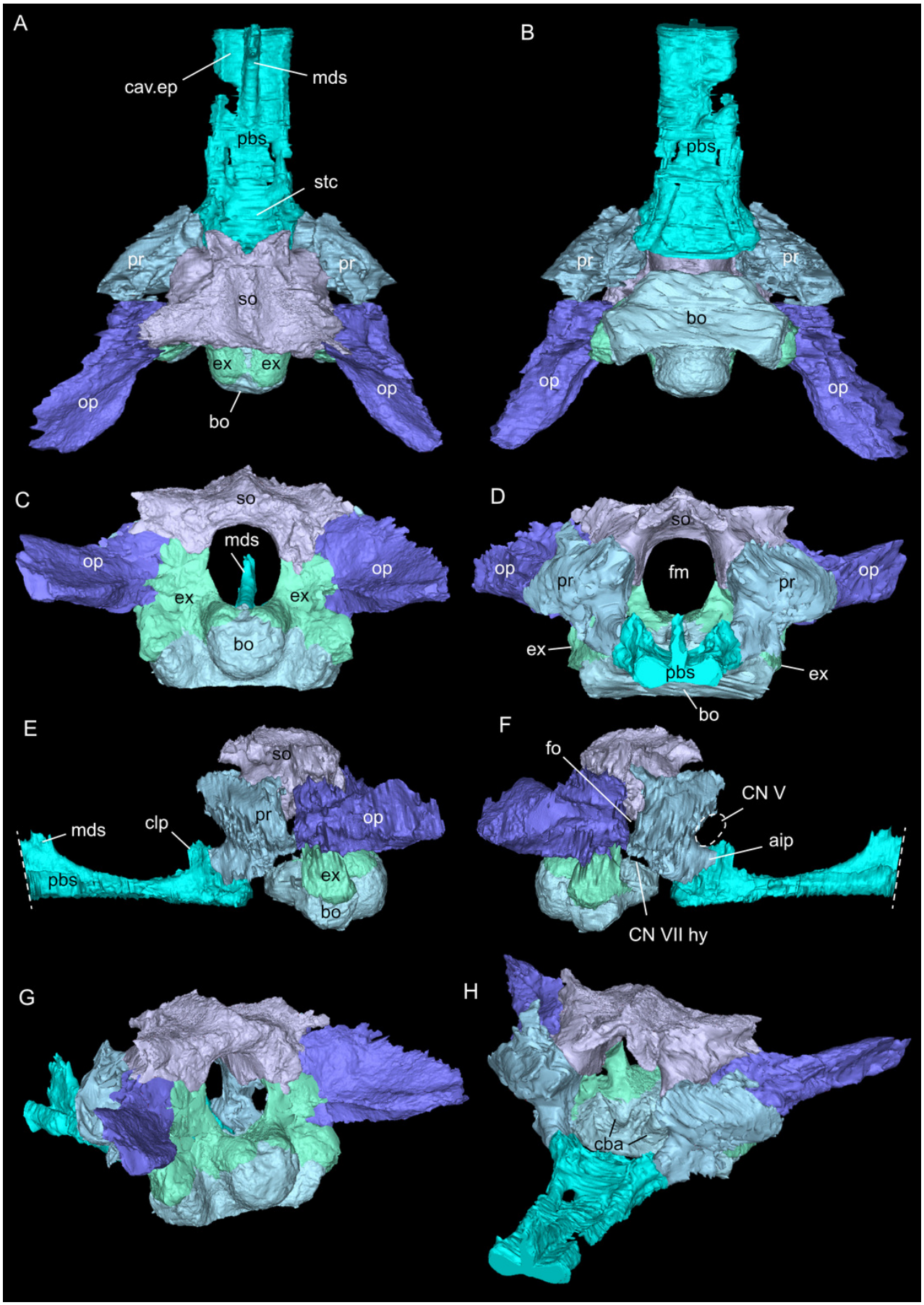
A
cav.ep
mds
pbs
stc
pr
pr
so
ex
ex
op
op
bo
B
pbs
pr
pr
bo
op
op
C
so
mds
op
op
ex
ex
bo
D
so
op
pr
fm
pr
op
ex
pbs
ex
bo
E
so
mds
clp
pr
op
pbs
ex
bo
F
fo
CN V
aip
CN VII hy
G
H
cba

Figure 6

Figure 6: Virtual rendering and segmentation of the floor of the braincase of *Simosaurus gaillardoti* (SMNS 16363).

Braincase floor elements in dorsal (A), ventral (B), left lateral (C), right lateral (D), angled left anterolateral (E), and dorsal view (F), the latter with segmented blood vessels shown. Elements not to scale.

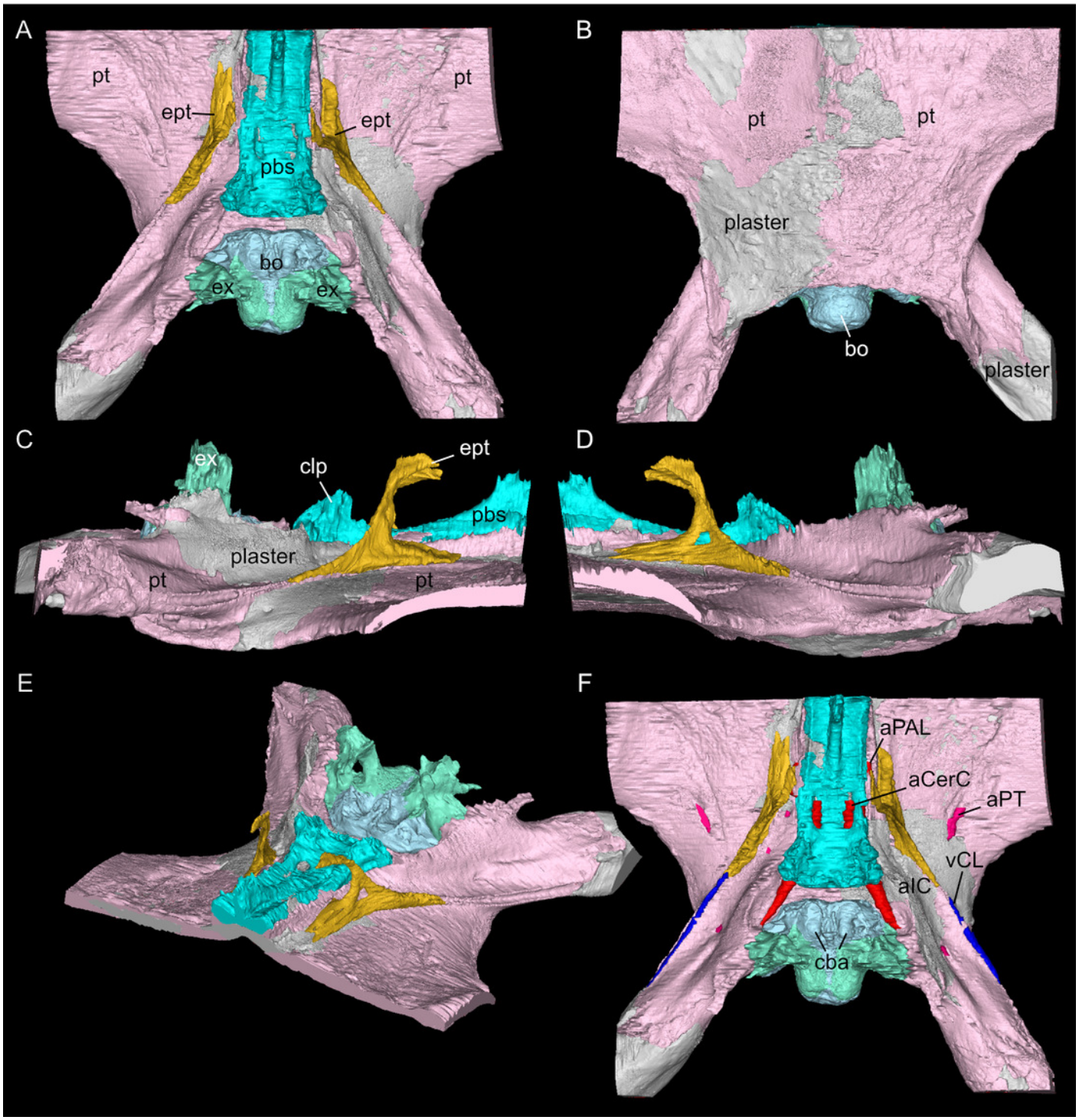
A
pt
pt
ept
ept
pbs
bo
ex
ex
B
pt
pt
plaster
bo
plaster
C
ex
clp
ept
pbs
plaster
pt
pt
D
E
F
aPAL
aCerC
aPT
vCL
aIC
cba

Figure 7

Figure 7: Segmented posterior cranial endocast and casts of blood vessels, nerves and bony labyrinth of *Simosaurus gaillardoti* (SMNS 16363) surrounded by selected transparent braincase bones.

Endocast and selected endocranial voids in dorsal (A), ventral (B), rostral (C), occipital (D), left lateral (E), and angled left posterolateral view (F). Elements not to scale.

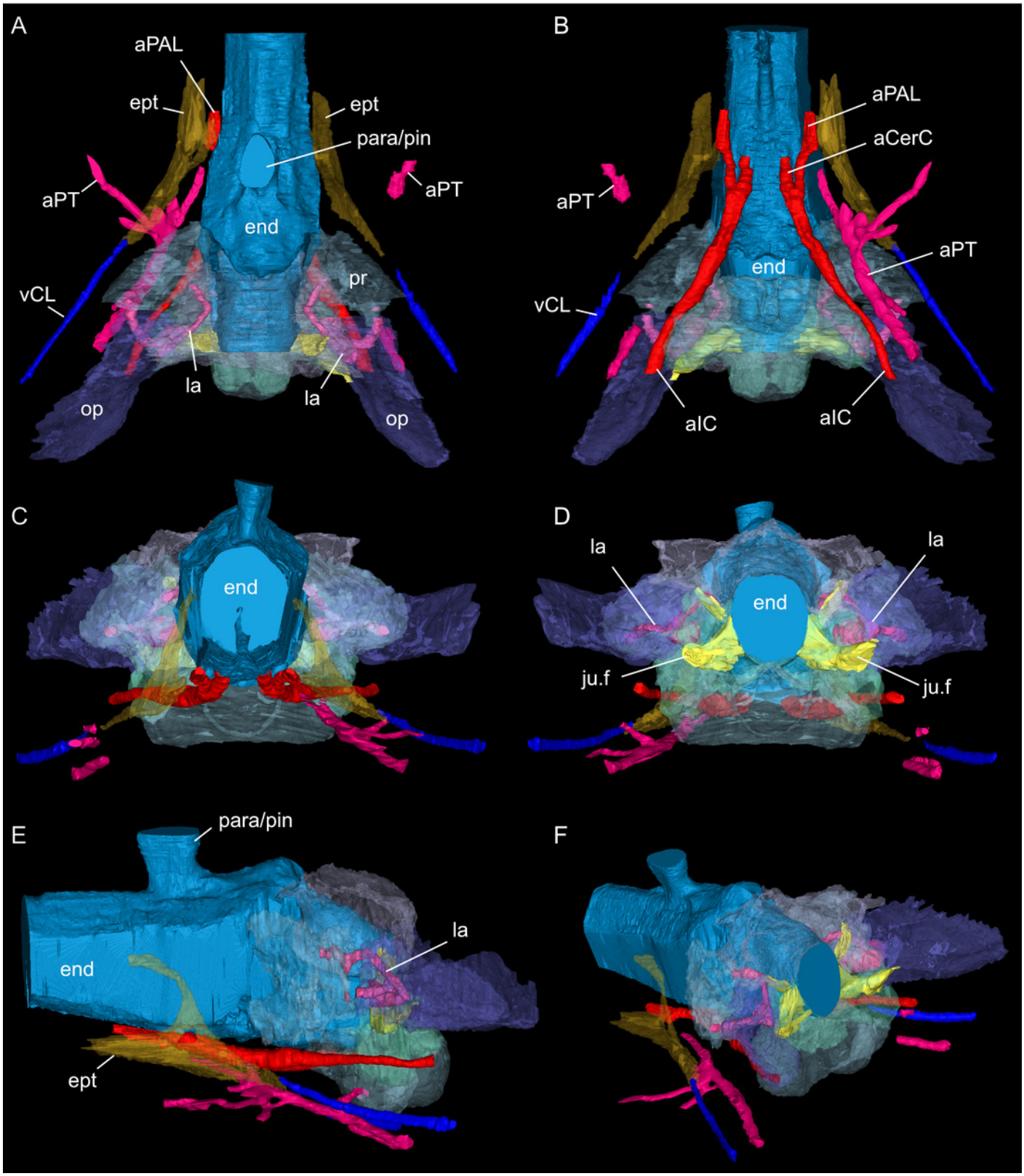
A
aPAL
ept
ept
para/pin
aPT
aPT
end
pr
vCL
la
la
op
op
B
aPAL
aCerC
aPT
aPT
end
vCL
aIC
aIC
C
end
D
la
la
end
ju.f
ju.f
E
para/pin
la
end
ept
F

Figure 8

Figure 8: Segmented posterior cranial endocast and selected cranial voids (blood vessels, nerves, bony labyrinth, and part of sinus system) of *Simosaurus gaillardoti* (SMNS 16363).

Endocast and selected endocranial voids in dorsal (A), ventral (B), rostral (C), angled left posterolateral (D) views. (E) Right bony labyrinth in medial view. (F) Isolated cranial endocast in dorsal view. Elements not to scale.

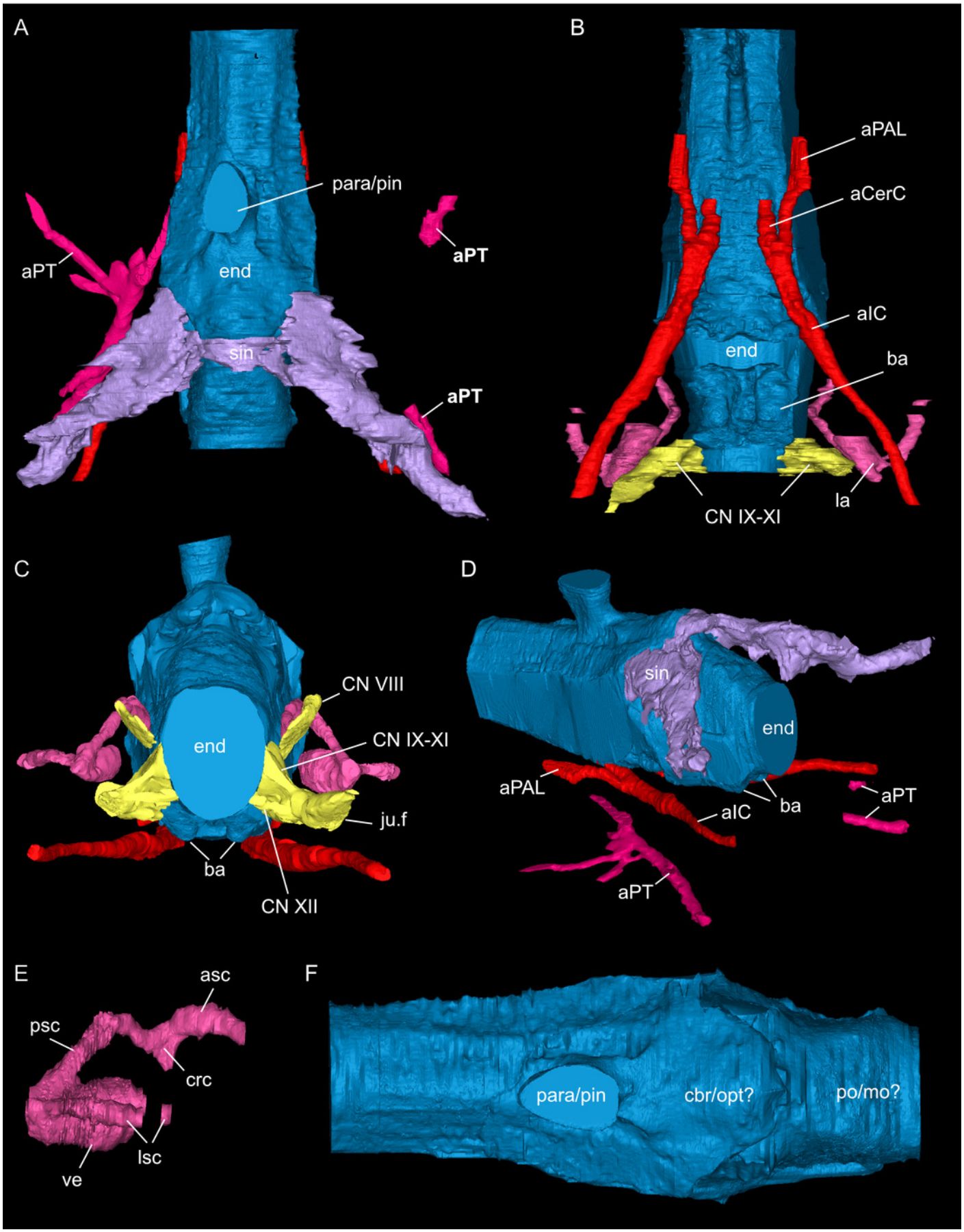
A
para/pin
aPT
aPT
end
sin
aPT
B
aPAL
aCerC
aIC
end
ba
CN IX-XI
la
C
CN VIII
end
CN IX-XI
ju.f
ba
CN XII
D
sin
end
aPAL
aIC
ba
aPT
aPT
E
asc
psc
crc
lsc
ve
F
para/pin
cbr/opt?
po/mo?

Figure 9

Figure 9: Segmented associated prootic, opisthotic and bony labyrinth (A-D), as well as right epipterygoid (E-J) of *Simosaurus gaillardoti* (SMNS 16363).

Inner ear region in occipital (A), rostral (B), ventral (C), and dorsal view. Right epipterygoid in lateral (E), medial (F), rostral (G), occipital (H), dorsal (I), and ventral (J) view. Elements not to scale.

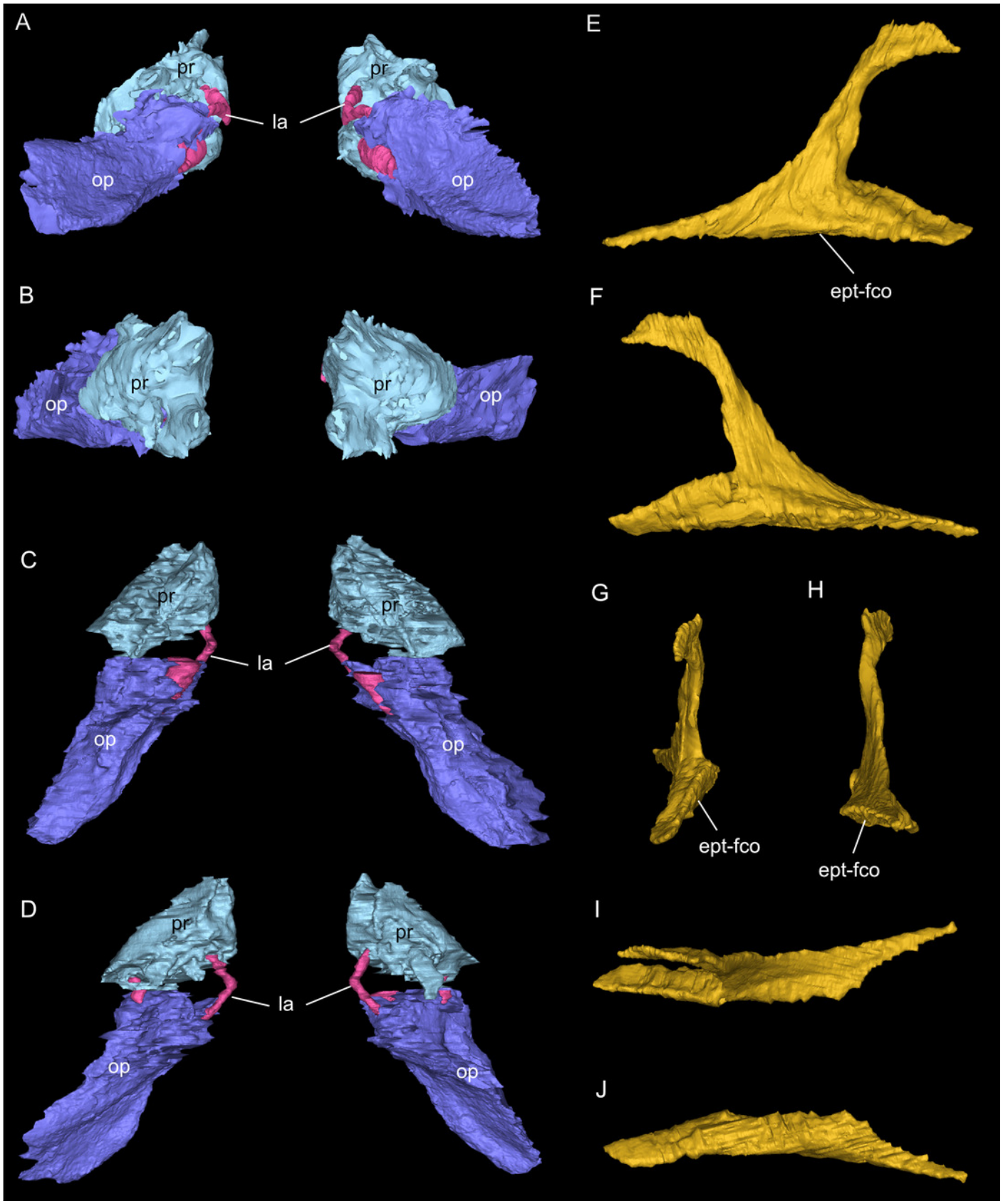
A
pr
la
op
pr
op
B
op
pr
pr
op
C
pr
la
op
pr
op
D
pr
la
op
pr
op
E
ept-fco
F
G
ept-fco
H
ept-fco
I
J

Figure 10

Figure 10: Comparison of segmented sauropterygian endocasts.

(A, B) *Simosaurus gaillardoti* SMNS 16363; this study; (C, D) *Placodus gigas* (UMO BT 13; modified after Neenan & Scheyer, 2012); (E, F) *Nothosaurus marchicus* (TW480000375; modified after Voeten et al., 2018); (G, H) *Libonectes morgani* (D1-8213, modified after Allemand et al., 2019). Note that the cranial endocast of *P. gigas* was mirrored to reflect the direction of the other endocasts (anterior is towards the left). Images in (A), (C), (E), and (G) show the endocasts in dorsal, images in (B), (D), (F), and (H) in lateral view. Passages for cranial nerves are indicated in yellow, blood vessels in dark red, and the bony labyrinth in lighter red/pink. Elements not to scale.

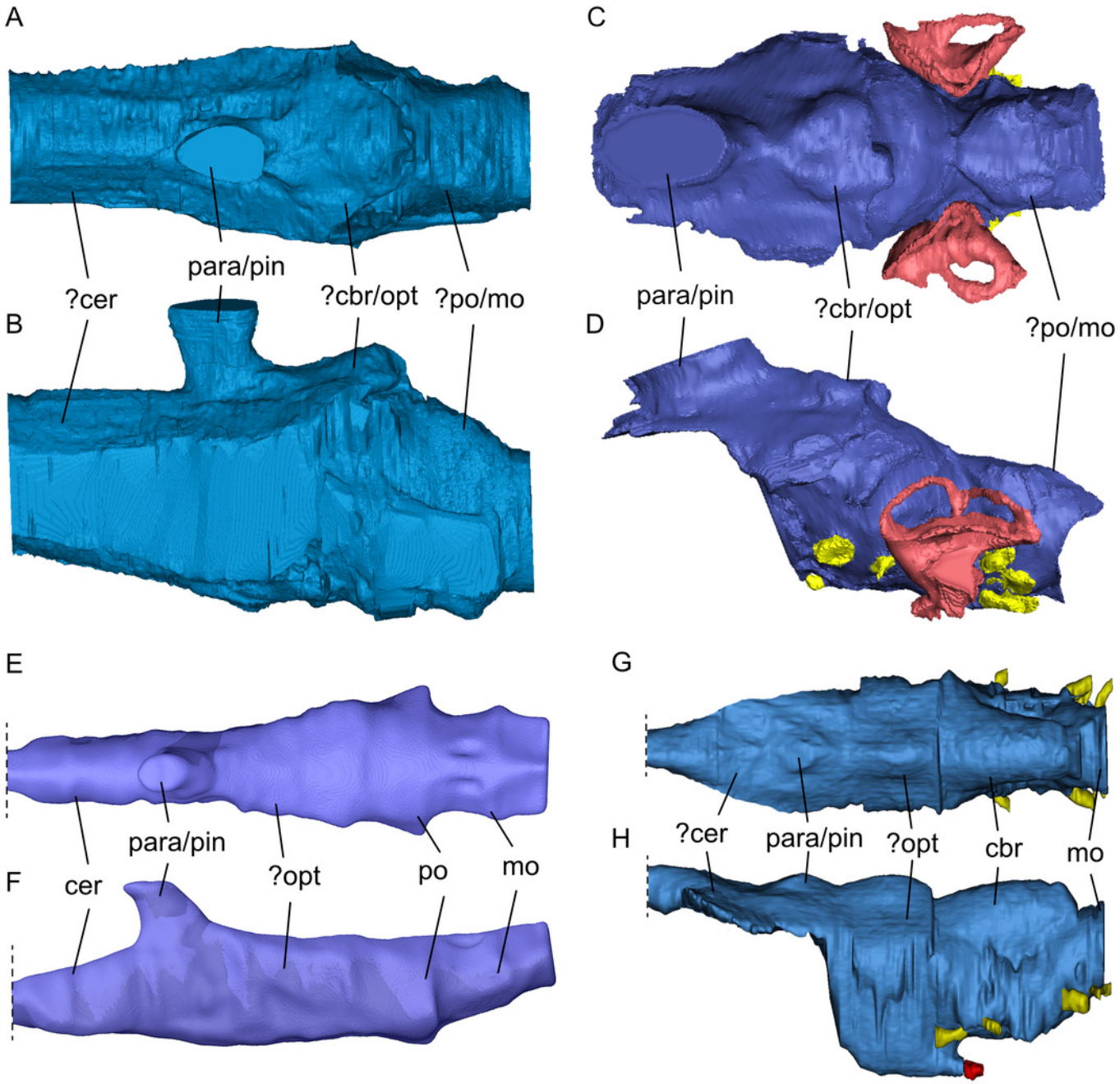
A
?cer
para/pin
?cbr/opt
?po/mo
B
C
para/pin
?cbr/opt
?po/mo
D
E
para/pin
?opt
po
mo
F
cer
G
?cer
para/pin
?opt
cbr
mo
H